Numerical Analysis of Retarded Potential Integral Equations of Electromagnetism

Sören Bartels

September 18, 1998

Contents

1 Electric and Magnetic Fields in Homogeneous Isotropic Media

In this section a short introduction to Maxwell's Equations is given. More details can be found in [AlFi], [Jo], [Wa].

1.1 Electrostatics

A region where an *electric charge* experiences a force is called an *electric field*. Such a region is for example produced by a point charge q positioned at $\mathbf{a} \in \mathbb{R}^3$. The resulting electric field at a point $\mathbf{x} \in \mathbb{R}^3 \setminus \{\mathbf{a}\}$ is then given by

$$\mathbf{E}(\mathbf{x}) = \frac{q}{4\pi\epsilon} \frac{\mathbf{x}-\mathbf{a}}{|\mathbf{x}-\mathbf{a}|^3}.$$

with ϵ being the permittivity of the medium.

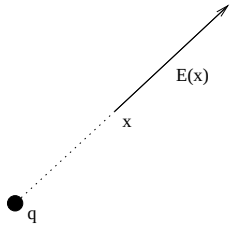

Figure 1: Electric field due to a positive charge q

Proposition 1 (Gauss' Law) *Let $\Omega \subset \mathbb{R}^3$ be a bounded Lipschitz–domain and $\mathbf{E}$ be the electric field produced by the charges $q_1, ..., q_k$ at $\mathbf{a_1}, ..., \mathbf{a_k} \in \mathbb{R}^3 \setminus \partial\Omega$, i.e.*

$$\mathbf{E}(\mathbf{x}) = \sum_{j=1}^{k} \frac{q_j}{4\pi\epsilon} \frac{\mathbf{x}-\mathbf{a_j}}{|\mathbf{x}-\mathbf{a_j}|^3}.$$

Then there holds Gauss' law

$$\int_{\partial\Omega} \mathbf{E} \cdot \mathbf{n}\, ds = \frac{1}{\epsilon} \sum_{\mathbf{a_j} \in \Omega} q_j.$$

Proof. It is clear that $\operatorname{div} \frac{\mathbf{x}-\mathbf{a_j}}{|\mathbf{x}-\mathbf{a_j}|^3} = 0$ for $\mathbf{x} \in \mathbb{R}^3 \setminus \{\mathbf{a_1}, ..., \mathbf{a_k}\}$. In the case $\mathbf{a_j} \notin \Omega, j = 1, ..., n$, the divergence–theorem can be applied directly to Ω and $\mathbf{E}$. In the case that only $\mathbf{a_1} \in \Omega$, choose a ball $\overline{B_r(\mathbf{a_1})} \subset \Omega$ and define $\Omega_{\mathbf{a_1}} := \Omega \setminus \overline{B_r(\mathbf{a_1})}$. The divergence–theorem can now be applied to $\Omega_{\mathbf{a_1}}$ and $\mathbf{E}$. This gives

$$\begin{aligned} 0 &= \int_{\Omega_{\mathbf{a_1}}} \operatorname{div} \mathbf{E}\, d\mathbf{x} \\ &= \int_{\partial\Omega_{\mathbf{a_1}}} \mathbf{E} \cdot \mathbf{n}\, ds \\ &= \int_{\partial\Omega} \mathbf{E} \cdot \mathbf{n}\, ds + \int_{\partial B_r(\mathbf{a_1})} \mathbf{E} \cdot \mathbf{n}\, ds. \end{aligned}$$

On $\partial B_r(\mathbf{a_1})$ it is $\mathbf{n}(\mathbf{x}) = -\frac{1}{r}(\mathbf{x}-\mathbf{a})$ which gives

$$\int_{\partial\Omega} \mathbf{E} \cdot \mathbf{n}\, ds = \frac{q_1}{4\pi\epsilon} \int_{\partial B_r(\mathbf{a_1})} \frac{|\mathbf{x}-\mathbf{a_1}|^2}{r|\mathbf{x}-\mathbf{a_1}|^3}\, ds = \frac{q_1}{4\pi\epsilon r^2} \int_{\partial B_r(\mathbf{a_1})} 1\, ds = \frac{q_1}{\epsilon}.$$

This proves the statement for $\mathbf{a_1} \in \Omega$ and the more general situation follows similarly.

Remark. The charge q can be taken as the contribution from a *charge density* ρ. In this case, the electric field is given by

$$\mathbf{E}(\mathbf{x}) = \frac{1}{4\pi\epsilon}\int_{D_\rho} \frac{\rho(\mathbf{y})\,(\mathbf{x}-\mathbf{y})}{|\mathbf{x}-\mathbf{y}|^3}\,d\mathbf{y},$$

where D_ρ is the domain of ρ. Gauss' law then becomes

$$\int_{\partial\Omega} \mathbf{E}\cdot\mathbf{n}\,ds = \int_\Omega \rho\,d\mathbf{x}.$$

Now consider the more general situation where charges are in steady motion. The *current flux* $\mathbf{j}$ is then defined as the charge that passes through a unit area per unit time, i.e.

$$\mathbf{j} = nq\mathbf{v},$$

where n is the number of particles, q the charge of the particles and $\mathbf{v}$ their velocity. *Ohm's law* says that that in a *conductor*, e.g. metal, the current flux is proportional to the electric field, i.e.

$$\mathbf{j} = \sigma\mathbf{E},$$

with σ being the *conductivity* of the medium. For *perfect conductors* the conductivity is taken to be equal to infinity, i.e. $\mathbf{E} = \mathbf{0}$.

1.2 Magnetostatics

Since magnetic bodies show interactions, it is reasonable to say that a magnetic body produces a *magnetic field*. Such a field is defined to be a region where a charge experiences a force only if it is in motion. Not only magnetic bodies produce these fields. When a current is present, the same field occurs. For a current flux $\mathbf{j}$ in a domain $D_\mathbf{j}$ the magnetic field $\mathbf{B}$ at $\mathbf{x}\in\mathbb{R}^3$ is given by

$$\mathbf{B}(\mathbf{x}) = \frac{\mu}{4\pi}\int_{D_\mathbf{j}} \frac{\mathbf{j}\times(\mathbf{x}-\mathbf{y})}{|\mathbf{x}-\mathbf{y}|^3}\,d\mathbf{y},$$

where μ is the magnetic permeability.

Example. Consider a very long rectilinear current I as shown in figure 2. Here I is the integral of the current flux $\mathbf{j}$ through a cross section S. Then for a point $\mathbf{x}\in\mathbb{R}^3$ at a distance r to the current a short calculation shows that

$$\mathbf{B}(\mathbf{x}) = \frac{\mu I}{4\pi r}\mathbf{t},$$

where $\mathbf{t}$ is the unit tangent vector to the perpendicular circle around I with radius r. This can be regarded as the force that acts on a wire containing a current at a distance r to I.

Proposition 2 (Ampère's Law I) *For a bounded Lipschitz-domain $\Omega\subset\mathbb{R}^3$ there holds* Ampère's law, *i.e.*

$$\int_{\partial\Omega} \mathbf{B}\cdot\mathbf{n}\,ds = 0.$$

Proof. It is

$$\begin{aligned}
\mathbf{B}(\mathbf{x}) &= \frac{\mu}{4\pi}\int_{D_\mathbf{j}} \frac{\mathbf{j}\times(\mathbf{x}-\mathbf{y})}{|\mathbf{x}-\mathbf{y}|^3}\,d\mathbf{y}\\
&= -\frac{\mu}{4\pi}\int_{D_\mathbf{j}} \mathbf{j}\times\operatorname{grad}\frac{1}{|\mathbf{x}-\mathbf{y}|}\,d\mathbf{y}\\
&= \frac{\mu}{4\pi}\operatorname{curl}\int_{D_\mathbf{j}} \frac{\mathbf{j}}{|\mathbf{x}-\mathbf{y}|}\,d\mathbf{y}.
\end{aligned}$$

Noting that $\operatorname{div}\operatorname{curl}\equiv 0$ the divergence–theorem gives the statement.

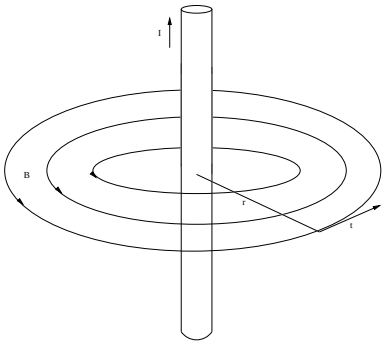

Figure 2: Magnetic field due to a rectilinear current

Proposition 3 (Ampère's Law II) *Let $S \subset \mathbb{R}^3$ be a surface bounded by the closed path L and assume that $\mathbf{j}$ is confined in $D_\mathbf{j}$, i.e. $\mathbf{j} \cdot \mathbf{n} = 0$ on $\partial D_\mathbf{j}$, and $\operatorname{div} \mathbf{j} = 0$ in $D_\mathbf{j}$. The magnetic circulation along the L is then*

$$\int_L \mathbf{B} \cdot dl = \mu \int_S \mathbf{j} \cdot \mathbf{n}\, ds.$$

Proof. It is

$$\begin{aligned}
\operatorname{div} \int_{D_\mathbf{j}} \frac{\mathbf{j}}{|\mathbf{x}-\mathbf{y}|}\, d\mathbf{y} &= \int_{D_\mathbf{j}} \mathbf{j} \cdot \operatorname{grad} \frac{1}{|\mathbf{x}-\mathbf{y}|}\, d\mathbf{y} \\
&= -\int_{D_\mathbf{j}} \mathbf{j} \cdot \operatorname{grad}_\mathbf{y} \frac{1}{|\mathbf{x}-\mathbf{y}|}\, d\mathbf{y} \\
&= -\int_{D_\mathbf{j}} \operatorname{div}_\mathbf{y} \frac{\mathbf{j}}{|\mathbf{x}-\mathbf{y}|}\, d\mathbf{y} \\
&= -\int_{\partial D_\mathbf{j}} \frac{\mathbf{j}}{|\mathbf{x}-\mathbf{y}|} \cdot \mathbf{n}\, ds_\mathbf{y} \\
&= 0,
\end{aligned}$$

where in the last equality the assumption that $\mathbf{j} \cdot \mathbf{n} = 0$ on $\partial D_\mathbf{j}$ was used. From the proof of Proposition 2 it follows that

$$\begin{aligned}
\operatorname{curl} \mathbf{B} &= \frac{\mu}{4\pi} \operatorname{curl} \left(\operatorname{curl} \int_{D_\mathbf{j}} \frac{\mathbf{j}}{|\mathbf{x}-\mathbf{y}|}\, d\mathbf{y} \right) \\
&= -\frac{\mu}{4\pi} \operatorname{div} \left(\operatorname{grad} \int_{D_\mathbf{j}} \frac{\mathbf{j}}{|\mathbf{x}-\mathbf{y}|}\, d\mathbf{y} \right) + \frac{\mu}{4\pi} \operatorname{grad} \left(\operatorname{div} \int_{D_\mathbf{j}} \frac{\mathbf{j}}{|\mathbf{x}-\mathbf{y}|}\, d\mathbf{y} \right) \\
&= \mu \mathbf{j}(\mathbf{x}),
\end{aligned}$$

where the fact that $\operatorname{div} \left(\operatorname{grad} \int_{D_h} \frac{h(\mathbf{y})}{|\mathbf{x}-\mathbf{y}|}\, d\mathbf{y} \right) = -4\pi h(\mathbf{x})$ for a continuous function h was used. Now, Stokes' theorem gives

$$\int_L \mathbf{B} \cdot dl = \int_S \operatorname{curl} \mathbf{B} \cdot \mathbf{n}\, ds = \mu \int_S \mathbf{j} \cdot \mathbf{n}\, ds.$$

1.3 Electromagnetic Induction

Consider an electric conductor that is represented by a smooth surface $S \subset \mathbb{R}^3$ such that S is bounded by a closed path L. Assume that this conductor is placed in a region where a time-dependent magnetic field exists. Then, by the principle of *electromagnetic induction*, a current may be observed. Experiments as shown in figure 3, where a time-dependent magnetic field $\mathbf{B}$ flows through the surface S, indicate that a

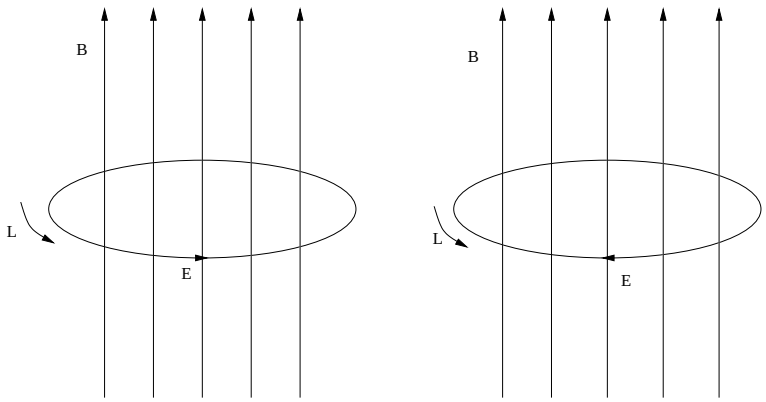

Figure 3: Electric field produced by a time–dependent magnetic field with $\frac{d}{dt}\int_S \mathbf{B}\cdot\mathbf{n}\,ds$ positive (left) and negative (right).

current occurs and that the circulation along L of the associated electric field is equal to the negative of the time rate of change of the magnetic flux through the surface S, i.e.

$$\int_L \mathbf{E}\cdot dl = -\frac{d}{dt}\int_S \mathbf{B}\cdot\mathbf{n}\,ds.$$

This is the *Faraday–Henry law* for electromagnetic induction.

1.4 Conservation of Charge and the Ampère–Maxwell Law

In the following, the basic assumption is that in all processes that occur in the universe, the net amount of charge never changes or equivalently, electric charge is conserved. Mathematically speaking, this means that for a region $\Omega \subset \mathbb{R}^3$, the time rate of change of charge must be equal to the difference of outgoing and incoming charge flux, i.e.

$$-\frac{dq}{dt} = \int_{\partial\Omega} \mathbf{j}\cdot\mathbf{n}\,ds.$$

Recalling Gauss' law for the electric field,

$$q = \epsilon\int_{\partial\Omega} \mathbf{E}\cdot\mathbf{n}\,ds,$$

one obtains the conservation law

$$\int_{\partial\Omega} \mathbf{j}\cdot\mathbf{n}\,ds + \epsilon\frac{d}{dt}\int_{\partial\Omega} \mathbf{E}\cdot\mathbf{n}\,ds = 0, \tag{1}$$

which becomes

$$\int_{\partial\Omega} \mathbf{j}\cdot\mathbf{n}\,ds = 0 \qquad \text{or} \qquad \operatorname{div}\mathbf{j} = 0$$

for the static case. Ampère's law II states that in this case for a surface S bounded by a closed path L the circulation of the magnetic field is given by

$$\int_L \mathbf{B}\cdot dl = \mu\int_S \mathbf{j}\cdot\mathbf{n}\,ds. \tag{2}$$

In section 1.2 it was illustrated that a current produces a magnetic field, thus one expects that in the situation of a time-dependent electric field, the magnetic field is no longer static. By comparing the conservation laws

for the static and time-dependent situation, Maxwell suggested to replace the right-hand-side of (2) by the term for the time-dependent case (1) and gave a physical explanation of the resulting equation

$$\int_L \mathbf{B}\cdot dl = \mu \int_S \mathbf{j}\cdot \mathbf{n}\, ds + \mu\epsilon \frac{d}{dt}\int_S \mathbf{E}\cdot \mathbf{n}\, ds,$$

the *Ampére–Maxwell law*. Experiments show that this law describes the situation correctly.

1.5 Maxwell's Equations in Integral Form

In the previous sections, the following integral–laws for electromagnetic fields in a domain $T \subset \mathbb{R}^3$ due to a charge–density ρ and a current–flux $\mathbf{j}$ were illustrated for bounded Lipschitz–domains $\Omega \subset T$ and smooth surfaces $S \subset T$ bounded by a closed path L:

$$\int_{\partial\Omega} \mathbf{E}\cdot \mathbf{n}\, ds = \frac{1}{\epsilon}\int_\Omega \rho\, d\mathbf{x}, \tag{3}$$

$$\int_{\partial\Omega} \mathbf{B}\cdot \mathbf{n}\, ds = 0, \tag{4}$$

$$\int_L \mathbf{E}\cdot dl = -\frac{d}{dt}\int_S \mathbf{B}\cdot \mathbf{n}\, ds, \tag{5}$$

$$\int_L \mathbf{B}\cdot dl = \mu \int_S \mathbf{j}\cdot \mathbf{n}\, ds + \mu\epsilon \frac{d}{dt}\int_S \mathbf{E}\cdot \mathbf{n}\, ds. \tag{6}$$

Although the first two equations describe static situations, the set of these four laws is in agreement with experimental data. They are called *Maxwell's Equations*.

1.6 Maxwell's Equations in Differential Form

Proposition 4 *For continuously differentiable vector–fields* $\{\mathbf{E}, \mathbf{B}\}$ *in* T *satisfying equations (3) -(6) for all* $S, \Omega \subset T$ *with a continuous vector–field* $\mathbf{j}$ *and an integrable function* ρ *it is*

$$\operatorname{div}\mathbf{E} = \frac{\rho}{\epsilon}, \tag{7}$$

$$\operatorname{div}\mathbf{B} = 0, \tag{8}$$

$$\operatorname{curl}\mathbf{E} + \frac{\partial}{\partial t}\mathbf{B} = 0, \tag{9}$$

$$\operatorname{curl}\mathbf{B} - \mu\epsilon\frac{\partial}{\partial t}\mathbf{E} = \mu\mathbf{j}. \tag{10}$$

Proof. For Gauss' and Ampère's law one can use the divergence theorem and let the volume of the region Ω tend to zero to obtain a differential form. This results in

$$\operatorname{div}\mathbf{E} = \frac{\rho}{\epsilon}.$$

Similarly, one gets

$$\operatorname{div}\mathbf{B} = 0.$$

For the Faraday–Henry and the Ampère–Maxwell law, Stokes' Theorem is helpful to get a differential form. It is

$$\int_L \mathbf{E}\cdot dl = \int_S \operatorname{curl}\mathbf{E}\cdot \mathbf{n}\, ds,$$

implying that

$$\int_S \left(\operatorname{curl}\mathbf{E} + \frac{\partial}{\partial t}\mathbf{B}\right)\cdot \mathbf{n}\, ds = 0.$$

Since this holds for arbitrary surfaces $S \subset \mathbb{R}^3$, it follows that

$$\operatorname{curl} \mathbf{E} + \frac{\partial}{\partial t}\mathbf{B} = 0.$$

the same procedure shows that

$$\operatorname{curl} \mathbf{B} - \mu\epsilon\frac{\partial}{\partial t}\mathbf{E} = \mu\mathbf{j}.$$

2 Analysis of Electromagnetic Fields

2.1 Electromagnetic Potentials

Lemma 1 *Let* $\mathbf{F}$ *be a continuously differentiable vector–field on* $\mathbb{R}^3$*. Then*

1. $\operatorname{curl}\mathbf{F} = \mathbf{0} \quad \Rightarrow \quad \mathbf{F} = \operatorname{grad} f$ *for a continuously differentiable function* f *on* $\mathbb{R}^3$,
2. $\operatorname{div}\mathbf{F} = 0 \quad \Rightarrow \quad \mathbf{F} = \operatorname{curl}\mathbf{G}$ *for a continuously differentiable vector–field* $\mathbf{G}$ *on* $\mathbb{R}^3$.

Proposition 5 *For smooth vector–fields* $\{\mathbf{E}, \mathbf{B}\}$ *satisfying the Maxwell–Equations in* $\mathbb{R}^3$ *there exists a function* ϕ *and a vector–field* $\mathbf{A}$ *such that*

$$\mathbf{B} = \operatorname{curl}\mathbf{A} \quad \textit{and} \quad \mathbf{E} = -\operatorname{grad}\phi - \frac{\partial \mathbf{A}}{\partial t}.$$

ϕ *and* $\mathbf{A}$ *can be chosen so that they satisfy the* Lorentz–Gauge condition

$$\operatorname{div}\mathbf{A} + \mu\epsilon\frac{\partial \phi}{\partial t} = 0$$

and are solutions of the wave equations

$$\begin{aligned} \Delta\phi - \mu\epsilon\frac{\partial^2\phi}{\partial t^2} &= -\frac{\rho}{\epsilon}, \\ \Delta\mathbf{A} - \mu\epsilon\frac{\partial^2\mathbf{A}}{\partial t^2} &= -\mu\mathbf{j}. \end{aligned}$$

Proof. By (8) and lemma 1 there exists a vector–field $\mathbf{A}$ such that the magnetic field $\mathbf{B}$ can be expressed as

$$\mathbf{B} = \operatorname{curl}\mathbf{A}.$$

Substituting this into (9) one gets

$$\operatorname{curl}\left(\mathbf{E} + \frac{\partial \mathbf{A}}{\partial t}\right) = 0,$$

and thus $\mathbf{E} + \frac{\partial \mathbf{A}}{\partial t}$ is equal to the gradient of a scalar function $-\phi$, i.e.

$$\mathbf{E} = -\operatorname{grad}\phi - \frac{\partial \mathbf{A}}{\partial t}.$$

For chosen $\mathbf{A}_0$ and ϕ_0, $\mathbf{A}_0$ can be, using the fact that the curl of a gradient is equal to zero, changed to $\mathbf{A} = \mathbf{A}_0 - \operatorname{grad}\psi$ for a scalar function ψ. To keep the representation for $\mathbf{B}$ and $\mathbf{E}$ valid, ϕ_0 has to be changed to $\phi = \phi_0 + \frac{\partial \psi}{\partial t}$.
Let ψ be a solution of the wave equation

$$\Delta\psi - \mu\epsilon\frac{\partial^2\psi}{\partial t^2} = \operatorname{div}\mathbf{A}_0 + \mu\epsilon\frac{\partial \phi_0}{\partial t}.$$

It is then

$$\begin{aligned} \operatorname{div}\mathbf{A} + \mu\epsilon\frac{\partial \phi}{\partial t} &= \operatorname{div}\mathbf{A}_0 - \operatorname{div}\operatorname{grad}\psi + \mu\epsilon\frac{\partial \phi_0}{\partial t} + \mu\epsilon\frac{\partial^2\psi}{\partial t^2} \\ &= \operatorname{div}\mathbf{A}_0 + \mu\epsilon\frac{\partial \phi_0}{\partial t} - \left(\Delta\psi - \mu\epsilon\frac{\partial^2\psi}{\partial t^2}\right) \\ &= 0. \end{aligned}$$

Now, (7) becomes

$$\begin{aligned}\frac{\rho}{\epsilon} &= \operatorname{div}\mathbf{E}\\ &= \operatorname{div}\left(-\operatorname{grad}\phi - \frac{\partial \mathbf{A}}{\partial t}\right)\\ &= -\Delta\phi + \mu\epsilon\frac{\partial^2}{\partial t^2}\phi,\end{aligned}$$

and, using that $\operatorname{curl}\operatorname{curl} = \operatorname{grad}\operatorname{div} - \Delta$,

$$\begin{aligned}\mu\mathbf{j} &= \operatorname{curl}\mathbf{B} - \mu\epsilon\frac{\partial \mathbf{E}}{\partial t}\\ &= \operatorname{curl}\operatorname{curl}\mathbf{A} + \mu\epsilon\frac{\partial}{\partial t}\operatorname{grad}\phi + \mu\epsilon\frac{\partial^2}{\partial t^2}\mathbf{A}\\ &= \operatorname{grad}\operatorname{div}\mathbf{A} - \Delta\mathbf{A} + \mu\epsilon\operatorname{grad}\frac{\partial}{\partial t}\phi + \mu\epsilon\frac{\partial^2}{\partial t^2}\mathbf{A}\\ &= \operatorname{grad}\left(\operatorname{div}\mathbf{A} + \mu\epsilon\frac{\partial}{\partial t}\phi\right) - \Delta\mathbf{A} + \mu\epsilon\frac{\partial^2}{\partial t^2}\mathbf{A}\\ &= -\Delta\mathbf{A} + \mu\epsilon\frac{\partial^2}{\partial t^2}\mathbf{A}.\end{aligned}$$

2.2 A Fundamental Solution for the three-dimensional Wave Equation

Consider the three-dimensional wave equation

$$\Delta p - \frac{1}{v^2}\frac{\partial^2 p}{\partial t^2} = -\delta_0.$$

To solve this for p in $\mathbb{R}^3 \setminus \{0\}$, one first notes that the problem is rotationally symmetric. Thus using polar-coordinates, the equation becomes

$$\frac{1}{R^2}\left(\frac{\partial}{\partial R}R^2\frac{\partial p}{\partial R}\right) - \frac{1}{v^2}\frac{\partial^2}{\partial t^2} = 0.$$

Using the transformation $U = p/R$, $\xi = t - R/v$ and $\eta = t + R/v$, one ends up with the simple partial differential equation

$$\frac{\partial^2 U}{\partial\xi\,\partial\eta} = 0.$$

A solution U has the form $U(\xi,\eta) = f(\xi) + g(\eta)$ for two arbitrary functions f, g. To prove this, note that $\partial_\eta U$ is independent of ξ and thus

$$U(\xi,\eta) = U(\xi,0) + \int_0^\eta \partial_\eta U(0,\eta')\,d\eta'.$$

Obviously,

$$U(\xi,0) = U(0,0) + \int_0^\xi \partial_\xi U(\xi',0)\,d\xi'$$

and so

$$U(\xi,\eta) = U(0,0) + \int_0^\eta \partial_\eta U(0,\eta')\,d\eta' + \int_0^\xi \partial_\xi U(\xi',0)\,d\xi',$$

which proves the statement. In terms of p and the variables $\mathbf{x}, t$ it is

$$p(\mathbf{x},t) = \frac{f(t - R/v)}{R} + \frac{g(t + R/v)}{R}$$

with $R = |\mathbf{x}|$. Since f represents an outgoing wave, g an incoming wave towards the origin, the g–term is not in agreement with physical observations and can therefore be neglected, i.e.

$$p(x,t) = \frac{f(t - R/v)}{R}.$$

Since a point source of unit strength for all time produces a static potential $1/(4\pi R)$ (compare section 1.1), one expects that a point source with the time-dependent strength $f(t)$ produces a potential $p = f(t - R/v)/(4\pi R)$. To obtain a fundamental solution, it is a good idea to replace f by δ_0, to get $p_1 = \delta_{t-R/v}/(4\pi R)$.

Theorem 1 *The map*

$$\varphi \to \int_{-\infty}^{+\infty} \left\langle \frac{\delta_{t-|\cdot|/v}}{4\pi|\cdot|}, \varphi(\cdot,t) \right\rangle dt, \qquad \varphi \in \mathcal{S}(\mathbb{R}^3 \times \mathbb{R}),$$

defines a tempered distribution E_+. Moreover E_+ is a fundamental solution for the three-dimensional wave equation.

Corollary. For an electromagnetic field $\mathbf{E}$ in $\mathbb{R}^3$, the potentials $\mathbf{A}$ and ϕ can be represented as follows

$$\mathbf{A}(\mathbf{x},t) = \frac{\mu}{4\pi} \int_{\mathbb{R}^3} \frac{\mathbf{j}(\mathbf{y}, t - \sqrt{\mu\epsilon}|\mathbf{x}-\mathbf{y}|)}{|\mathbf{x}-\mathbf{y}|}\, d\mathbf{y}$$

and

$$\phi(\mathbf{x},t) = \frac{1}{4\pi\epsilon} \int_{\mathbb{R}^3} \frac{\rho(\mathbf{y}, t - \sqrt{\mu\epsilon}|\mathbf{x}-\mathbf{y}|)}{|\mathbf{x}-\mathbf{y}|}\, d\mathbf{y}.$$

A short calculation shows that $\mathbf{A}$ and ϕ satisfy the Lorentz–Gauge condition

$$\operatorname{div} \mathbf{A} + \mu\epsilon \frac{\partial \phi}{\partial t} = 0.$$

2.3 Continuity–Properties of Electromagnetic Fields across the Interface of two different Media

In this section the basic assumption is that the Faraday–Henry law

$$\int_L \mathbf{E} \cdot dl = -\frac{d}{dt} \int_S \mathbf{B} \cdot \mathbf{n}\, ds$$

is still valid when two different media are considered, but no assumptions about continuity of $\mathbf{E}$ or $\mathbf{B}$ across the interface between the media are made.

Proposition 6 *Let $\{\mathbf{E}, \mathbf{B}\}$ be an electromagnetic field in $\Omega_1 \cup \Omega_2$, $\Omega_1, \Omega_2 \subset \mathbb{R}^3$ representing two different media, such that $\overline{\Omega_1 \cup \Omega_2} = \mathbb{R}^3$ and the interface between Ω_1 and Ω_2 is smooth. If $\mathbf{E}(\cdot,t)$ is continuous and $\frac{\partial}{\partial t}\mathbf{B}(\cdot,t)$ is bounded in $\overline{\Omega_i}$, $i = 1,2$ for all $t \in \mathbb{R}_{>0}$, then the tangential component of the electric field is continuous across the interface.*

Proof. Let $t \in \mathbb{R}$ be fixed and let $\mathbf{x_0}$ be a point on the interface between Ω_1 and Ω_2 and let $\epsilon \in \mathbb{R}_{>0}$. Then there exist δ_1 and δ_2 such that

$$|\mathbf{E}(\mathbf{x}) - \mathbf{E^i}(\mathbf{x_0})| < \epsilon \quad \text{for all } \mathbf{x} \in B_{\delta_i}(\mathbf{x_0}) \cap \overline{\Omega_i}, \quad i = 1,2,$$

where $\mathbf{E^i}(\mathbf{x_0})$ denotes the limit approaching $\mathbf{x_0}$ from Ω_i. Let $\mathbf{n}$ be a normal and $\mathbf{t}$ be a tangent to the interface at $\mathbf{x_0}$ and choose a rectangle L with sides of length δ_s and δ_l parallel to $\mathbf{n}$ and $\mathbf{t}$ sucht that $L \subset B_\delta(\mathbf{x_0})$, where $\delta = \min(\delta_1, \delta_2)$ (compare figure 4). Let S denote the interior plane bounded by L. Then it is

$$\begin{aligned} \int_L \mathbf{E} \cdot dl &= \int_A \mathbf{E} \cdot \mathbf{t}\, ds - \int_{A'} \mathbf{E} \cdot \mathbf{t}\, ds + \int_B \mathbf{E} \cdot \mathbf{n}\, ds - \int_{B'} \mathbf{E} \cdot \mathbf{n}\, ds \\ &= \int_A (\mathbf{E}(\mathbf{x}) - \mathbf{E}(\mathbf{x} - \delta_l \mathbf{n})) \cdot \mathbf{t}\, ds + \int_B (\mathbf{E}(\mathbf{x}) - \mathbf{E}(\mathbf{x} - \delta_s \mathbf{t})) \cdot \mathbf{n}\, ds \end{aligned}$$

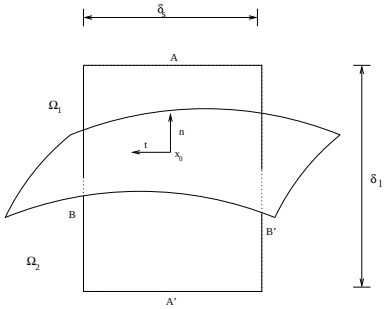

Figure 4: Loop through the interface between Ω_1 and Ω_2

and

$$\left|\frac{d}{dt}\int_S \mathbf{B}\cdot\mathbf{n}\,ds\right| \le \left\|\frac{\partial}{\partial t}\mathbf{B}\right\|_{\sup(S)} \delta_s\delta_l.$$

It follows that

$$\begin{aligned}
\left|\int_A (\mathbf{E}(\mathbf{x}) - \mathbf{E}(\mathbf{x}-\delta_l\mathbf{n}))\cdot\mathbf{t}\,ds\right| &\le \left\|\frac{\partial}{\partial t}\mathbf{B}\right\|_{\sup(S)} \delta_s\delta_l + \int_B |\mathbf{E}(\mathbf{x}) - \mathbf{E}(\mathbf{x}-\delta_s\mathbf{t})|\,ds \\
&\le \left\|\frac{\partial}{\partial t}\mathbf{B}\right\|_{\sup(S)} \delta_s\delta_l + \int_B \big(\big|\mathbf{E}(\mathbf{x}) - \mathbf{E^2}(\mathbf{x_0})\big| \\
&\quad + \big|\mathbf{E^1}(\mathbf{x_0}) - \mathbf{E}(\mathbf{x}-\delta_s\mathbf{t})\big| + \big|\mathbf{E^2}(\mathbf{x_0}) - \mathbf{E^1}(\mathbf{x_0})\big|\big)\,ds \\
&\le \left\|\frac{\partial}{\partial t}\mathbf{B}\right\|_{\sup(S)} \delta_s\delta_l + \big(2\epsilon + |\mathbf{E^2}(\mathbf{x_0}) - \mathbf{E^1}(\mathbf{x_0})|\big)\,\delta_l.
\end{aligned}$$

Now divide by δ_s, choose $\delta_s := \sqrt{\delta_l}$ and take the limit $\delta_l \to 0$.

Remark. By choosing a small cylinder through the interface it can be shown that the normal component of the magnetic field is continuous across the interface.

2.4 Scattered Fields from Surfaces

Let $\Gamma \subset \mathbb{R}^3$ be a closed surface representing a perfect conductor such that $\Gamma = \partial\Omega$ for a bounded Lipschitz–domain $\Omega \subset \mathbb{R}^3$. Let $\mathbf{E}^{inc}$ be an incident electric field in $\Omega' := \mathbb{R}^3 \setminus \overline{\Omega}$ which reaches Γ at $t = 0$. The incident field causes a surface current $\mathbf{j}$ and a surface charge ρ on Γ. These quantities are assumed to be identically zero for times $t \le 0$. For times $t > 0$ they will produce a *scattered* electric field $\mathbf{E}^{scat}$ in Ω'. The field $\mathbf{E}^{scat}$ satisfies the Maxwell–Equations in Ω', with associated magnetic field $\mathbf{B}$ and, by linearity, the total field $\mathbf{E}^{tot} = \mathbf{E}^{scat} + \mathbf{E}^{inc}$ satisfies the Maxwell–Equations in Ω', too. Thus the tangential component of $\mathbf{E}^{tot}$ is continuous across Γ. Since Γ is assumed to be a perfect conductor, the tangential component has to be zero. This gives the boundary condition

$$0 = \left[\mathbf{E}^{tot}\right]_{tan} = \left[\mathbf{E}^{scat} + \mathbf{E}^{inc}\right]_{tan},$$

or

$$\left[\mathbf{E}^{scat}\right]_{tan} = -\left[\mathbf{E}^{inc}\right]_{tan} \text{ on } \Gamma.$$

Furthermore, the *radiation condition*

$$|\mathbf{E}^{scat}(\mathbf{x},t)| \to 0, \quad |\mathbf{x}| \to \infty, \quad t > 0 \tag{11}$$

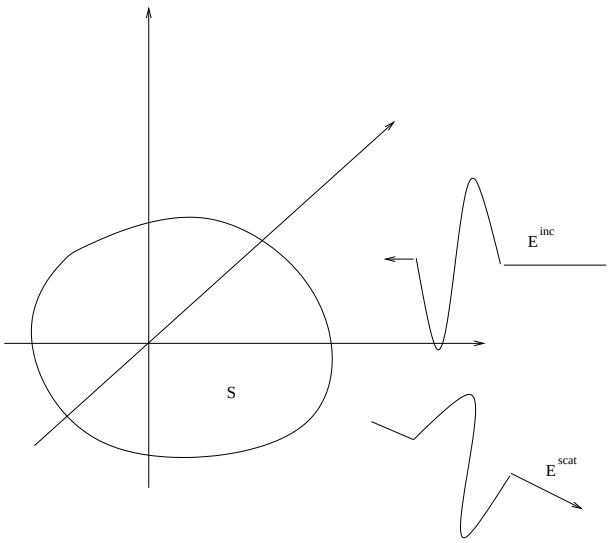

Figure 5: Incident and scattered field from a surface S

has to be imposed. $\{\mathbf{E}^{scat}, \mathbf{B}\}$ is thus a solution of the exterior problem

$$\left.\begin{array}{rcll} \operatorname{curl}\mathbf{E}^{scat} + \frac{\partial}{\partial t}\mathbf{B} &=& \mathbf{0}, & \\ -\mu\epsilon\frac{\partial}{\partial t}\mathbf{E}^{scat} + \operatorname{curl}\mathbf{B} &=& \mathbf{0}, & \\ \operatorname{div}\mathbf{E}^{scat} = \operatorname{div}\mathbf{B} &=& 0 \quad \text{in} \quad \Omega' \times \mathbb{R}_{>0} & \\ \mathbf{E}^{scat} = \mathbf{B} &=& 0, \quad t \leq 0, & \\ [\mathbf{E}^{scat}]_{tan} &=& -\left[\mathbf{E}^{inc}\right]_{tan} \text{ on } \Gamma \times \mathbb{R}_{>0}, & \\ |\mathbf{E}^{scat}(\mathbf{x},t)| &\to& 0, \quad |\mathbf{x}| \to \infty, \quad t > 0. & \end{array}\right\} (P_{\Omega'})$$

The field $\{\mathbf{E}^{scat}, \mathbf{B}\}$ can be extended to Ω such that it is a solution of the interior problem

$$\left.\begin{array}{rcll} \operatorname{curl}\mathbf{E}^{scat} + \frac{\partial}{\partial t}\mathbf{B} &=& \mathbf{0}, & \\ -\mu\epsilon\frac{\partial}{\partial t}\mathbf{E}^{scat} + \operatorname{curl}\mathbf{B} &=& \mathbf{0}, & \\ \operatorname{div}\mathbf{E}^{scat} = \operatorname{div}\mathbf{B} &=& 0 \quad \text{in} \quad \Omega \times \mathbb{R}, & \\ \mathbf{E}^{scat} = \mathbf{B} &=& 0, \quad t \leq 0, & \\ [\mathbf{E}^{scat}]_{tan} &=& -\left[\mathbf{E}^{inc}\right]_{tan} \text{ on } \Gamma \times \mathbb{R}_{>0}. & \end{array}\right\} (P_{\Omega})$$

Theorem 2 *For smooth solutions $\{\mathbf{E}^{scat}, \mathbf{B}\}$ of (P_Ω) and $(P_{\Omega'})$ it is*

$$\mathbf{E}^{scat}(\mathbf{x},t) = -\frac{1}{4\pi\epsilon}\frac{\partial}{\partial t}\int_\Gamma \frac{\mathbf{j}(\mathbf{y}, t-\sqrt{\mu\epsilon}|\mathbf{x}-\mathbf{y}|)}{|\mathbf{x}-\mathbf{y}|}\,ds_{\mathbf{y}} - \frac{\mu}{4\pi}\operatorname{grad}\int_\Gamma \frac{\rho(\mathbf{y}, t-\sqrt{\mu\epsilon}|\mathbf{x}-\mathbf{y}|)}{|\mathbf{x}-\mathbf{y}|}\,ds_{\mathbf{y}}, \tag{12}$$

$t \in \mathbb{R}_{>0}$, $\mathbf{x} \notin \Gamma$, and

$$\mathbf{B}(\mathbf{x},t) = \frac{1}{4\pi\epsilon}\operatorname{curl}\int_\Gamma \frac{\mathbf{j}(\mathbf{y}, t-\sqrt{\mu\epsilon}|\mathbf{x}-\mathbf{y}|)}{|\mathbf{x}-\mathbf{y}|}\,ds_{\mathbf{y}}, \tag{13}$$

$t \in \mathbb{R}_{>0}$, $\mathbf{x} \notin \Gamma$, where ρ is the jump of $-\mathbf{n}\cdot\mathbf{E}^{scat}$ and $\mathbf{j}$ the jump of $-\mathbf{n}\times\mathbf{B}$ across Γ. ρ and $\mathbf{j}$ are related by the equation of conservation of charge, i.e.

$$\frac{\partial}{\partial t}\rho + \operatorname{div}_\Gamma \mathbf{j} = 0,$$

where $\operatorname{div}_\Gamma$ is the surface divergence operator with respect to Γ (see below). By continuity, $\mathbf{E}^{scat}$ can be extended to Γ.

Remark. The problems (P_Ω) and $(P_{\Omega'})$ can now be condensed to the following set of equations: Given $\mathbf{E}^{inc}$, find ρ, $\mathbf{j}$ such that

$$\frac{\partial}{\partial t}\rho + \operatorname{div}_\Gamma \mathbf{j} = 0$$

and

$$\left[\mathbf{E}^{scat}\right]_{tan} = -\left[\mathbf{E}^{inc}\right]_{tan} \text{ on } \Gamma,$$

where $\mathbf{E}^{scat}$ is the electric field defined by (12).

Remark. Scattered fields also occur from open surfaces Γ. In this situation, it is assumed that Γ can be extended to a closed surface, i.e. there exists a bounded Lipschitz–domain $\Omega \subset \mathbb{R}^3$ such that $\Gamma = \Gamma \cap \partial\Omega$. The representation formula can then be derived for $\partial\Omega$ but the jumps of $\mathbf{n}\cdot\mathbf{E}$ and $\mathbf{n}\times\mathbf{B}$ across $\partial\Omega$ are zero on $\partial\Omega \setminus \Gamma$, so that the integration has only to be carried out on Γ. This means that (12) is still valid when Γ is an open surface. In order to keep the equation of conservation of charge valid, the condition that the current flows along the edge of Γ, or

$$\mathbf{j}\cdot\tilde{\mathbf{n}} = 0 \text{ on } \partial\Gamma, \tag{14}$$

where $\tilde{\mathbf{n}} = -\mathbf{n}\times\mathbf{t}$, has to be imposed.

Remark. Setting

$$\mathbf{A}(\mathbf{x},t) := \frac{1}{4\pi\epsilon}\int_\Gamma \frac{\mathbf{j}(\mathbf{y}, t-\sqrt{\mu\epsilon}|\mathbf{x}-\mathbf{y}|)}{|\mathbf{x}-\mathbf{y}|}\, ds_{\mathbf{y}} \tag{15}$$

and

$$\phi(\mathbf{x},t) := \frac{\mu}{4\pi}\int_\Gamma \frac{\rho(\mathbf{y}, t-\sqrt{\mu\epsilon}|\mathbf{x}-\mathbf{y}|)}{|\mathbf{x}-\mathbf{y}|}\, ds_{\mathbf{y}}, \tag{16}$$

(12) becomes $\mathbf{E}^{scat} = -\operatorname{grad}\phi - \frac{\partial}{\partial t}\mathbf{A}$, i.e. a similar expression as for electromagnetic fields in $\mathbb{R}^3$. It can be shown that $\mathbf{A}$ and ϕ also satisfy the Lorentz-Gauge condition $\operatorname{div}\mathbf{A} + \mu\epsilon\frac{\partial}{\partial t}\phi = 0$.

2.5 Functionalanalytic Framework

In order to define operators associated to the representation formula (12) the following defintions are needed. Let $\Omega \subset \mathbb{R}^3$ be a bounded Lipschitz–domain and $\Gamma = \partial\Omega$. The spaces $L^2(\Omega)$, $H^{1/2}(\Gamma)$ and $H^{-1/2}(\Gamma)$ are assumed to be known (or see for example [A]).

Definition 1 *The spaces $H(curl,\Omega)$ and $H(div,\Omega)$ are defined as*

$$\begin{aligned} H(curl,\Omega) &:= \{\mathbf{v}\in L^2(\Omega)^3; \operatorname{curl}\mathbf{v}\in L^2(\Omega)^3\},\\ H(div,\Omega) &:= \{\mathbf{v}\in L^2(\Omega)^3; \operatorname{div}\mathbf{v}\in L^2(\Omega)\}, \end{aligned}$$

where $\operatorname{curl}\mathbf{v}\in L^2(\Omega)^3$ if there exists $\mathbf{p}\in L^2(\Omega)^3$ such that

$$\int_\Omega \mathbf{p}\phi\, d\mathbf{x} = \int_\Omega \mathbf{v}\cdot\operatorname{curl}\phi\, d\mathbf{x} \qquad (\phi\in C_0^1(\Omega)^3)$$

and $\operatorname{div}\mathbf{v}\in L^2(\Omega)$ if there exists $p\in L^2(\Omega)$ such that

$$\int_\Omega p\phi\, d\mathbf{x} = -\int_\Omega \mathbf{v}\cdot\nabla\phi\, d\mathbf{x} \qquad (\phi\in C_0^1(\Omega)).$$

$H(curl,\Omega)$ and $H(div,\Omega)$ are equipped with the inner–products

$$\begin{aligned} <\mathbf{u},\mathbf{v}>_{H(curl,\Omega)} &:= \int_\Omega \mathbf{u}\cdot\mathbf{v}\, d\mathbf{x} + \int_\Omega \operatorname{curl}\mathbf{u}\cdot\operatorname{curl}\mathbf{v}\, d\mathbf{x}\\ <\mathbf{u},\mathbf{v}>_{H(div,\Omega)} &:= \int_\Omega \mathbf{u}\cdot\mathbf{v}\, d\mathbf{x} + \int_\Omega \operatorname{div}\mathbf{u}\operatorname{div}\mathbf{v}\, d\mathbf{x}. \end{aligned}$$

Remark. $H(curl,\Omega)$ and $H(div,\Omega)$ are Hilbert–spaces.

Definition 2 *Let* $\mathbf{u}$ *be a smooth tangent vector–field on* Γ. *The* surface curl, $\operatorname{curl}_\Gamma \mathbf{u}$, *is defined as*

$$\operatorname{curl}_\Gamma \mathbf{u} := \mathbf{n} \cdot \operatorname{curl} \tilde{\mathbf{u}},$$

where $\tilde{\mathbf{u}}$ *is a regular extension of* $\mathbf{u}$ *to an open neighbourhood* U *of* Γ. *The* surface divergence, $\operatorname{div}_\Gamma \mathbf{u}$, *of* $\mathbf{u}$ *is the scalar*

$$\operatorname{div}_\Gamma \mathbf{u} := \operatorname{curl}_\Gamma (\mathbf{u} \times \mathbf{n})$$

while the tangential gradient, $\operatorname{grad}_\Gamma f$, *of a scalar function* f *on* Γ *is defined by*

$$< \operatorname{grad}_\Gamma f, \phi >_{L^2(\Gamma)^3} := < f, \operatorname{div}_\Gamma \phi >_{L^2(\Gamma)} \qquad (\phi \in C^1(\Gamma)^3).$$

Definition 3 *The trace spaces* $H^{-1/2}(\operatorname{div}, \Gamma)$ *and* $H^{-1/2}(\operatorname{curl}, \Gamma)$ *are defined as*

$$\begin{aligned} H^{-1/2}(\operatorname{div}, \Gamma) &= \{\mathbf{u} \in H^{-1/2}(\Gamma)^3; \quad \mathbf{u} \cdot \mathbf{n} = 0, \quad \operatorname{div}_\Gamma \mathbf{u} \in H^{-1/2}(\Gamma)\}, \\ H^{-1/2}(\operatorname{curl}, \Gamma) &= \{\mathbf{u} \in H^{-1/2}(\Gamma)^3; \quad \mathbf{u} \cdot \mathbf{n} = 0, \quad \operatorname{curl}_\Gamma \mathbf{u} \in H^{-1/2}(\Gamma)\} \end{aligned}$$

and are equipped with the norms $\|\cdot\|^2_{-1/2,div} = \|\cdot\|^2_{-1/2} + \|\operatorname{div}_\Gamma \cdot\|^2_{-1/2}$ *and* $\|\cdot\|^2_{-1/2,curl} = \|\cdot\|^2_{-1/2} + \|\operatorname{curl}_\Gamma \cdot\|^2_{-1/2}$.

Remark. $H^{-1/2}(\operatorname{div}, \Gamma)$ and $H^{-1/2}(\operatorname{curl}, \Gamma)$ are Hilbert–spaces.

Let E be an arbitrary Hilbert–space.

Definition 4 *The* Fourier–Laplace transformed $\hat{f}$ *of an* E*–valued function* $f \in L^1(\mathbb{R}, E)$ *is defined as*

$$\hat{f}(\omega) := \int_{-\infty}^{\infty} e^{i\omega t} f(t)\, dt, \qquad \omega \in \mathbb{C}.$$

Remark. Like the usual Fourier transformation, the Fourier–Laplace-transformation can be defined for distribution–spaces.

Definition 5 *For* $s \in \mathbb{R}$, $\sigma \in \mathbb{R}_{>0}$, *the space* $H^s_\sigma(\mathbb{R}_{>0}, E)$ *is the set of all* E*–valued distributions* f *with support in* $\mathbb{R}_{>0}$ *such that*

$$e^{-\sigma t} \Lambda^s f \in L^2(\mathbb{R}, E),$$

where the operator Λ^s *is defined for the Fourier–Laplace transformed of* f *by*

$$(\Lambda^s f)\hat{}\,(\omega) = (-i\omega)^s \hat{f}(\omega), \qquad \omega \in \mathbb{C}.$$

$H^s_\sigma(\mathbb{R}_{>0}, E)$ *is equipped with the norm*

$$|f|_{\sigma,s,E} := \left(\int_{-\infty}^{\infty} e^{-2i\sigma t} \|\Lambda^s f\|^2_E \, dt \right)^{1/2}.$$

Remark. For $E = H^{-1/2}(\operatorname{div}, \Gamma), H^{-1/2}(\operatorname{curl}, \Gamma), H^{1/2}(\Gamma), H^{-1/2}(\Gamma)$ write $|\cdot|_{\sigma,s,-1/2\operatorname{div}}, |\cdot|_{\sigma,s,-1/2\operatorname{curl}}, |\cdot|_{\sigma,s,1/2}, |\cdot|_{\sigma,s,-1/2}$.

2.6 Variational Formulation for the Retarded Potential Integral Equation

Let $\Omega \subset \mathbb{R}^3$ be a bounded Lipschitz–domain and $\Gamma = \partial\Omega$. The definition of the surface potentials $\mathbf{A}$ and ϕ leads to the introduction of the boundary integral operator

$$S\psi(x,t) := \int_\Gamma \frac{\psi(y, t - |x-y|)}{|x-y|}\, ds_y$$

for smooth functions ψ on $\Gamma \times \mathbb{R}_{>0}$. The *retarded potential integral equation* reads as follows:

$$\left.\begin{array}{l} \text{Given a function } g \text{ on } \Gamma \times \mathbb{R}_{>0}, \text{ find } \rho \text{ on } \Gamma \times \mathbb{R}_{>0} \\ \text{such that} \quad g = S\rho. \end{array}\right\} \text{(RPIE)}$$

For solutions $\{\mathbf{E}, \mathbf{B}\}$ of (P_Ω), $(P_{\Omega'})$, the surface potentials $\mathbf{A}$ and ϕ satisfy homogeneous wave equations in Ω and Ω'. Here, only the scalar potential ϕ will be considered. ϕ satisfies the interior wave problem

$$\left.\begin{array}{rcl} \Delta - \partial_t^2 u &=& 0 \text{ in } \mathbb{R}_{>0} \times \Omega \\ u(\cdot, 0) &=& 0 \text{ in } \Omega \\ \partial_t u(\cdot, 0) &=& 0 \text{ in } \Omega \\ u &=& g \text{ on } \Gamma \times \mathbb{R}_{>0}, \end{array}\right\} (Q_\Omega)$$

as well as the exterior wave problem

$$\left.\begin{array}{rcl} \Delta - \partial_t^2 u &=& 0 \text{ in } \mathbb{R}_{>0} \times \Omega' \\ u(\cdot, 0) &=& 0 \text{ in } \Omega' \\ \partial_t u(\cdot, 0) &=& 0 \text{ in } \Omega' \\ u &=& g \text{ on } \Gamma \times \mathbb{R}_{>0}, \end{array}\right\} (Q_{\Omega'})$$

for an appropriate choice of the boundary data g. Carrying out a temporal Fourier–Laplace transformation of these wave problems, one obtains that for all $\omega \in \mathbb{C}$, $\hat{\phi}(\omega, \cdot)$ is the solution of the Helmholtz–equations

$$\left.\begin{array}{rcl} \hat{u}(\omega, \cdot) &\in& H^1(\Omega) \\ (\Delta + \omega^2)\hat{u}(\omega, \cdot) &=& 0 \quad \text{in } \Omega \\ \hat{u}(\omega, \cdot) &=& \hat{g}(\omega, \cdot) \quad \text{on } \Gamma \end{array}\right\} (Q_\Omega^\omega)$$

and

$$\left.\begin{array}{rcl} \hat{u}(\omega, \cdot) &\in& H^1(\Omega') \\ (\Delta + \omega^2)\hat{u}(\omega, \cdot) &=& 0 \quad \text{in } \Omega' \\ \hat{u}(\omega, \cdot) &=& \hat{g}(\omega, \cdot) \quad \text{on } \Gamma. \end{array}\right\} (Q_{\Omega'}^\omega)$$

It is well–known that for $\operatorname{Im}\omega > 0$ the operator N_ω, which maps the Dirichlet–datum $\hat{g}(\omega, \cdot)$ to the jump of the normal derivative of the uniquely existing solution $\hat{u}(\omega, \cdot)$ across Γ,

$$N_\omega \hat{g}(\omega, \cdot) = \left[\frac{\partial \hat{u}}{\partial \mathbf{n}}(\omega, \cdot)\right]_\Gamma,$$

defines a bounded isomorphism from $H^{1/2}(\Gamma)$ to $H^{-1/2}(\Gamma)$. The inverse of N_ω is the operator S_ω, defined by

$$S_\omega \hat{\rho}(\omega, \mathbf{x}) := \int_\Gamma \frac{e^{i\omega|\mathbf{x}-\mathbf{y}|}}{|\mathbf{x}-\mathbf{y}|} \hat{\rho}(\omega, \mathbf{y})\, ds_{\mathbf{y}} \qquad \mathbf{x} \in \Gamma,$$

which is the Fourier–Laplace transformed of the operator S. By applying an inverse transformation to S_ω, Bamberger and Duong state in [BaDuo] the following theorems.

Theorem 3 *If $g \in H^{3/2}_{\sigma_0}(\mathbb{R}_{>0}, H^{1/2}(\Gamma))$ for some $\sigma_0 > 0$, then the problems (Q_Ω), $(Q_{\Omega'})$ have unique solutions $u \in H^0_{\sigma_0}(\mathbb{R}_{>0}, \overset{1}{H}(\Omega) \cup H^1(\Omega'))$. The solution u is uniquely representable by a retarded potential on Γ. The density ρ of that potential, $\rho = \left[\frac{\partial u}{\partial n}\right]_\Gamma$, satisfies*

$$|\rho|_{\sigma,-1/2,-1/2} \le C \frac{1}{\sigma} \max\left(\frac{1}{\sigma_0}, 1\right) |g|_{\sigma,3/2,1/2}, \qquad (\sigma \ge \sigma_0 > 0).$$

Theorem 4 *S is a bounded linear operator from $H^1_\sigma(\mathbb{R}_{>0}, H^{-1/2}(\Gamma))$ into $H^0_\sigma(\mathbb{R}_{>0}, H^{1/2}(\Gamma))$ satisfying the operator–norm inequality*

$$\int_{-\infty}^{\infty} e^{-2\sigma t} |S\rho(t)|^2_{1/2}\, dt \le C \frac{1}{\sigma_0^2} \max\left(\frac{1}{\sigma_0^4}, 1\right) \int_0^\infty e^{-2\sigma t} |\partial_t \rho(t)|^2_{-1/2}\, dt.$$

If ρ belongs to

$$D(S) = \{\psi \in H^1_\sigma(\mathbb{R}_{>0}, H^{-1/2}(\Gamma)), S\psi \in H^1_\sigma(\mathbb{R}_{>0}, H^{1/2}(\Gamma))\},$$

then there holds the coercivity–inequality

$$\int_{-\infty}^{\infty} e^{-2\sigma t} < \rho(t), S\left(\partial_t \rho(t)\right) > \, dt \ge C \min(\sigma_0, 1) |\rho|^2_{\sigma_0,-1/2,-1/2}.$$

This theorem allows to replace the problem of solving the retarded integral equation

$$g = S\rho$$

for given g by the following variational formulation:

$$\left.\begin{array}{l} \text{Find} \quad \rho \in H^1_\sigma(\mathbb{R}_{>0}, H^{-1/2}(\Gamma)) \quad \text{such that} \\ a(\rho,\psi) = b(\psi) \qquad (\psi \in H^1_\sigma(\mathbb{R}_{>0}, H^{-1/2}(\Gamma))), \end{array}\right\} \text{(VarRPIE)}$$

where

$$a(\rho,\psi) := \int_{-\infty}^{\infty} e^{-2\sigma t} \left(\int_\Gamma \int_\Gamma \frac{\psi(\mathbf{x},t)\partial_t \rho(\mathbf{y}, t-|\mathbf{x}-\mathbf{y}|)}{|\mathbf{x}-\mathbf{y}|}\, ds_{\mathbf{x}}\, ds_{\mathbf{y}} \right) dt \tag{17}$$

and

$$b(\psi) := \int_{-\infty}^{\infty} e^{-2\sigma t} \int_\Gamma \psi(\mathbf{x},t)\partial_t g(\mathbf{x},t)\, ds_{\mathbf{x}}\, dt. \tag{18}$$

2.7 Variational Formulation for the Electric Field Integral Equation

Instead of first formulating a wave problem for the surface potentials, Pujols applies in [Pu] the Fourier–Laplace transformation directly to the problems (P_Ω) and $(P_{\Omega'})$. By an inverse transformation he obtains results for an operator which allows to formulate the problem of solving the electric field integral equation as a varitional one.
The full problem, i.e. (P_Ω) and $(P_{\Omega'})$, can be formulated as follows: Given an incident field $\mathbf{E}^{inc}$ find the surface current $\mathbf{j}$ and the surface charge ρ such that $\mathbf{j}$ and ρ satisfy the equation of conservation of charge and

$$\left[\mathbf{E}^{scat}\right]_{tan} = -\left[\mathbf{E}^{inc}\right]_{tan} \quad \text{on} \quad \Gamma,$$

where $\mathbf{E}^{scat}$ is the scattered electric field defined by (12). Since ρ is assumed to be zero at $t = 0$, the equation of conservation of charge,

$$\frac{\partial \rho}{\partial t} + \operatorname{div}_\Gamma \mathbf{j} = 0,$$

can be rewritten as

$$\rho(\mathbf{x},t) = \int_0^t \operatorname{div}_\Gamma \mathbf{j}(\mathbf{x},s)\, ds.$$

This manipulation allows to remove ρ from the representation formula (12) and to define the boundary integral operator R which maps the current to the tangential component of the associated electric field, i.e.

$$R\mathbf{j}(\mathbf{x},t) = \left[-\frac{1}{4\pi\epsilon}\frac{\partial}{\partial t} S\mathbf{j}(\mathbf{x},t) - \frac{\mu}{4\pi} \operatorname{grad}_\Gamma S \left(\int_0^t \operatorname{div}_\Gamma \mathbf{j}(\mathbf{x},s)\, ds \right) \right]_{tan}, \qquad \mathbf{x} \in \Gamma.$$

The *electric field integral equation* reads as follows:

$$\left.\begin{array}{l} \text{Given an incident electric field } \mathbf{E}^{inc} \text{ find the surface current } \mathbf{j} \\ \text{such that} \quad R\mathbf{j} = -\left[\mathbf{E}^{inc}\right]_{tan} \text{ on } \Gamma. \end{array}\right\} \text{(EFIE)}$$

Pujols states the following theorem.

Theorem 5 *The pseudodifferential operator R is a bounded linear operator from $H^2_\sigma(\mathbb{R}_{>0}, H^{-1/2}(\operatorname{div}, \Gamma))$ to $H^0_\sigma(\mathbb{R}_{>0}, H^{-1/2}(\operatorname{curl}, \Gamma))$. The operator R allows to define a bilinear form which satisfies the coercivity inequality*

$$\int_0^\infty e^{-2\sigma t} < \mathbf{p}(t,\cdot), R\mathbf{p}(t,\cdot) > \, dt \geq C|\mathbf{p}|^2_{\sigma,-1,-1/2\operatorname{div}}.$$

This statement enables to express the full problem as a variational formulation.

$$\left.\begin{array}{l}\text{Given an incident field } \mathbf{E}^{inc} \text{ such that } \left[\mathbf{E}^{inc}\right]_{tan} \in H^0_\sigma(\mathbb{R}_{>0}, H^{-1/2}(\mathrm{curl}\,,\Gamma)),\\ \text{find } \mathbf{j} \in H^2_\sigma(\mathbb{R}_{>0}, H^{-1/2}(\mathrm{div}\,,\Gamma)) \text{ such that for all } \mathbf{p} \in H^1_\sigma(\mathbb{R}_{>0}, H^{-1/2}(\mathrm{div}\,,\Gamma))\\ a_2(\mathbf{p},\mathbf{j}) = b_2(\mathbf{p}),\end{array}\right\} \text{(VarEFIE)}$$

where

$$a_2(\mathbf{p},\mathbf{j}) := \int_0^\infty e^{-2\sigma t} < \mathbf{p}(t,\cdot), R\mathbf{j}(t,\cdot) > \, dt \tag{19}$$

and

$$b_2(\mathbf{p}) := -\int_0^\infty e^{-2\sigma t} < \mathbf{p}(t,\cdot), \mathbf{E}^{inc}_{tan}(t,\cdot) > \, dt. \tag{20}$$

3 Numerical Investigations for the scalar Retarded Potential Integral Equation

In calculating scattered fields, solving the retarded potential integral equation is part of the problem. Algorithms for solving this equation turn out to be very often unstable. In the following, two basic algorithms are introduced and their stability–properties analysed and compared.

3.1 Collocation Method

In this section the retarded potential integral equation is solved directly following a method Davies and Duncan use in [DaDu] for squares. Assume that g is a given function in space and time, P a smooth surface in $\mathbb{R}^3$ and consider the nondimensionalised retarded potential integral equation

$$g(\mathbf{x},t) = \int_P \frac{u(\mathbf{y}, t-|\mathbf{x}-\mathbf{y}|)}{|\mathbf{x}-\mathbf{y}|}\, ds_{\mathbf{y}},$$

which has to be solved for u. The surface P is discretized regularly into flat triangles $T \in \mathcal{T}$ and u is approximated by a function U that is piecewise constant in space and piecewise affine linear in time for a uniform discretization in time of size Δt, i.e.

$$U(\mathbf{x},t) = \sum_{T\in\mathcal{T}} \chi_T(\mathbf{x}) u_T(t),$$

where $\chi_T(\mathbf{x}) = 1$ if $\mathbf{x} \in T$, $\chi_T(\mathbf{x}) = 0$ otherwise, and

$$u_T(t) := \sum_{i=0}^{N} u_T^i \psi_i(t),$$

with ψ_i being the nodal basis functions in time, i.e. $\psi_i(j\Delta t) = \delta_{ij}$, and an appropriate choice for N so that the solution is approximated in the time interval $[0, N\Delta t]$. This approximation is substituted into the equation which is then tested at midpoints $\mathbf{x}_{T'}$ of triangles $T' \in \mathcal{T}$ and integer multiples of Δt, $t^n := n\Delta t$. This gives

$$\begin{aligned}
g(x_{T'}, t^n) &= \sum_{S\in\mathcal{T}} \int_S \sum_{T\in\mathcal{T}} \frac{\chi_T(\mathbf{x}_{T'}) u_T(t^n - |\mathbf{x}_{T'}-\mathbf{y}|)}{|\mathbf{x}_{T'}-\mathbf{y}|}\, ds_{\mathbf{y}} \\
&= \sum_{T\in\mathcal{T}} \int_T \frac{u_T(t^n - |\mathbf{x}_{T'}-\mathbf{y}|)}{|\mathbf{x}_{T'}-\mathbf{y}|}\, ds_{\mathbf{y}} \\
&= \sum_{T\in\mathcal{T}\setminus T'} \int_T \frac{u_T(t^n - |\mathbf{x}_{T'}-\mathbf{y}|)}{|\mathbf{x}_{T'}-\mathbf{y}|}\, ds_{\mathbf{y}} + \int_{T'} \frac{u_{T'}(t^n - |\mathbf{x}_{T'}-\mathbf{y}|)}{|\mathbf{x}_{T'}-\mathbf{y}|}\, ds_{\mathbf{y}}.
\end{aligned}$$

The integrals in the sum are approximated by the midpoint rule. Let Φ_T be the affine–linear transformation mapping the triangle $T_{ref} = \mathrm{conv}\,[(0,0),(1,0),(0,1)]$ to T. It is then

$$\begin{aligned}
\int_T \frac{u_T(t^n - |\mathbf{x}_{T'}-\mathbf{y}|)}{|\mathbf{x}_{T'}-\mathbf{y}|}\, ds_{\mathbf{y}} &= \int_{T_{ref}} \frac{u_T(t^n - |\mathbf{x}_{T'}-\Phi_T(\mathbf{y})|)}{|\mathbf{x}_{T'}-\Phi_T(\mathbf{y})|} \mathrm{gram}\,\Phi_T\, ds_{\mathbf{y}} \\
&\approx \frac{1}{2} \frac{u_T(t^n - |\mathbf{x}_{T'}-\Phi_T(\mathbf{x}_{T_{ref}})|)}{|\mathbf{x}_{T'}-\Phi_T(\mathbf{x}_{T_{ref}})|} \mathrm{gram}\,\Phi_T,
\end{aligned}$$

where $\mathrm{gram}\,\Phi_T := \sqrt{\det((D\Phi_T)^t D\Phi_T)}$ is the Gram determinant of Φ_T. The *selfpatch–integral* is treated as follows:

$$\int_{T'} \frac{u_{T'}(t^n - |\mathbf{x}_{T'}-\mathbf{y}|)}{|\mathbf{x}_{T'}-\mathbf{y}|}\, ds_{\mathbf{y}} = \int_{T_{ref}} \frac{u_{T'}(t^n - |\mathbf{x}_{T'}-\Phi_{T'}(\mathbf{y})|)}{|\mathbf{x}_{T'}-\Phi_{T'}(\mathbf{y})|} \mathrm{gram}\,\Phi_{T'}\, ds_{\mathbf{y}}$$

$$\begin{aligned} &\approx u_{T'}(t^n - |\mathbf{x}_{T'} - \Phi_{T'}(\mathbf{x}_{T_{ref}})|) \int_{T_{ref}} \frac{1}{|\mathbf{x}_{T'} - \Phi_{T'}(\mathbf{y})|} \operatorname{gram} \Phi_{T'}\, ds_{\mathbf{y}} \\ &= u_{T'}(t^n) \int_{T_{ref}} \frac{1}{|\mathbf{x}_{T'} - \Phi_{T'}(\mathbf{y})|} \operatorname{gram} \Phi_{T'}\, ds_{\mathbf{y}} \end{aligned}$$

where $\Phi_{T'}(1/3, 1/3) = \mathbf{x}_{T'}$ was used. These approximations lead to the equation

$$C_{T',T'} u_{T'}(t^n) = g(\mathbf{x}_{T'}, t^n) - \sum_{T \in \mathcal{T} \setminus T'} C_{T',T} u_T(t^n - |\mathbf{x}_{T'} - \Phi_T(1/3, 1/3)|), \tag{21}$$

where

$$C_{T',T'} = \operatorname{gram} \Phi_{T'} \int_{T_{ref}} \frac{1}{|\mathbf{x}_{T'} - \Phi_{T'}(\mathbf{y})|}\, ds_{\mathbf{y}} \quad \text{and} \quad C_{T',T} = \frac{\operatorname{gram} \Phi_T}{2|\mathbf{x}_{T'} - \mathbf{x}_T|}.$$

The terms $u_T(t^n - |\mathbf{x}_{T'} - \mathbf{x}_T|)$ are evaluated using the affine linearity of u_T between integer multiples of the time–step Δt, i.e.

$$u_T(t^n - |\mathbf{x}_{T'} - \mathbf{x}_T|) = (1 - \epsilon_{T',T}) u_T((n - m_{T',T})\Delta t) + \epsilon_{T',T} u_T((n - m_{T',T} - 1)\Delta t),$$

where

$$m_{T',T} = \lfloor |\mathbf{x}_{T'} - \mathbf{x}_T| / \Delta t \rfloor \quad \text{and} \quad \epsilon_{T,T'} = |\mathbf{x}_{T'} - \mathbf{x}_T| / \Delta t - m_{T,T'},$$

with $\lfloor \cdot \rfloor$ giving the integer part of a real number closest $-\infty$. Substituting these manipulations into (21) gives

$$C_{T',T'} u^n_{T'} = g(\mathbf{x}_{T'}, n\Delta t) - \sum_{T \in \mathcal{T} \setminus T_j} C_{T',T}((1 - \epsilon_{T',T}) u_T^{n - m_{T',T}} + \epsilon_{T',T} u_T^{n - m_{T',T} - 1}).$$

The scheme can now be written in matrix notation, that is testing at all midpoints $\{\mathbf{x}_T\}_{T \in \mathcal{T}}$ simultaneously. Using the initial condition $U = 0$ at $t = 0$ and writing $\mathbf{u}^n = (u^n_{T_j})_{j=1,\ldots,|\mathcal{T}|}$, $\mathbf{g}^n = (g(\mathbf{x}_{T_j}, t^n))_{j=1,\ldots,|\mathcal{T}|}$ one obtains the scheme

$$Q^0 \mathbf{u}^n = \mathbf{g}^n - \sum_{m=1}^{n-1} Q^m \mathbf{u}^{n-m}, \tag{22}$$

where

$$Q^m(j,k) = \sum_{m_{T_j,T_k} = m} C_{T_j,T_k}(1 - \epsilon_{T_j,T_k}) + \sum_{m_{T_j,T_k} = m-1} C_{T_j,T_k} \epsilon_{T_j,T_k}, \quad \text{if } m \neq 0,$$

$$Q^0(j,k) = \begin{cases} C_{T_j,T_k}, & \text{if } j = k, \\ \sum_{m_{T_j,T_k} = 0} C_{T_j,T_k}(1 - \epsilon_{T_j,T_k}), & \text{else.} \end{cases}$$

The matrix Q^0 is diagonal, if the *mesh ratio* $r := \min_{T_1,T_2 \in \mathcal{T}, T_1 \neq T_2} \Delta t / |\mathbf{x}_{T_1} - \mathbf{x}_{T_2}|$ is less than one, so that the scheme is explicit for $r < 1$. The matrices Q^m represent different *time–levels*, i.e. the domain of influence in calculating a specific value, is decomposed into rings at different past–times.
As an example take $P = [0,1]^2 \times \{0\}$ and $g(\mathbf{x}, t) = \exp(-10(t - 2.5)^2)$. P is discretized uniformly into halfed squares of size h. In figure 7 the logarithm of the L^2–norm of the numerical solution is plotted against time for different mesh ratios while the behaviour of the analytical solution is shown in figure 6. For most mesh ratios the norm of the numerical solution grows exponentially which indicates instability. In contrast to the results obtained by Duncan and Davies in [DaDu] for squares, where the algorithm is stable for mesh ratios $r \in]0.65, 1]$, no stability prediction can be made for triangles. It is interesting to see that the instability is regular, i.e. the solution differs $+/-$ on two triangles of a square (compare figure 8). Averaging methods can be introduced, to remove these instabilities.

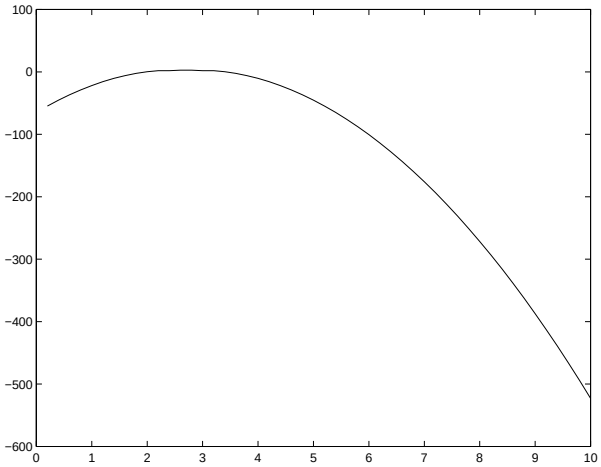

Figure 6: Logarithm of the L^2–norm of the analytical solution for $g(\mathbf{x},t) = \exp(-10(t-2.5)^2)$

3.2 Galerkin–Ansatz

Theorem 4 states that the retarded potential integral equation is associated with a coercive bilinear form. For a Galerkin–Ansatz a discrete subspace $V_{\mathcal{T},\Delta t}$ of $H^s_\sigma(\mathbb{R}_{>0}, H^{-1/2}(P))$ has to be chosen. As for the direct approach, take the space of functions that are piecewise constant in space and affine–linear, globally continuous in time for a regular triangulation $\mathcal{T}$ of P into flat triangles and a uniform discretization of time of size Δt, i.e.

$$V_{\mathcal{T},\Delta t} = \left\{ f; \quad f(\mathbf{x},t) = \sum_{T\in\mathcal{T}} \sum_{n=0}^{N} c_T^n \psi_n(t)\chi(\mathbf{x}), (c_T^n)_{T\in\mathcal{T},0\le n\le N} \in \mathbb{R}^{\mathcal{T}\times(N+1)} \right\}.$$

The discretized surface is denoted by $\tilde{P} := \bigcup_{T\in\mathcal{T}} T$. The bilinear form (17) discretizes as follows: Let $f \in V_{\mathcal{T},\Delta t}$ with coefficients (c_T^n) and let $c_T(t) := \sum_{n=0}^N c_T^n \psi(t)$. By linearity, it suffices to calculate $a(\psi_n\chi_{T'}, f)$. It is

$$\begin{aligned}
a(\psi_n\chi_{T'}, f) &= \int_0^\infty e^{-2\sigma t} \int_{\tilde{P}}\int_{\tilde{P}} \frac{\chi_{T'}(\mathbf{x})\psi_n(t)\partial_t f(\mathbf{y}, t-|\mathbf{x}-\mathbf{y}|)}{|\mathbf{x}-\mathbf{y}|}\, ds_{\mathbf{y}}\, ds_{\mathbf{x}}\, dt \\
&\approx 2\Delta t e^{-2\sigma t^n} \int_{\tilde{P}}\int_{\tilde{P}} \frac{\chi_{T'}(\mathbf{x})\psi_n(t^n)\partial_t f(\mathbf{y}, t^n-|\mathbf{x}-\mathbf{y}|)}{|\mathbf{x}-\mathbf{y}|}\, ds_{\mathbf{y}}\, ds_{\mathbf{x}} \\
&= 2\Delta t e^{-2\sigma t^n} \int_{\tilde{P}}\int_{\tilde{P}} \frac{\chi_{T'}(\mathbf{x})\partial_t f(\mathbf{y}, t^n-|\mathbf{x}-\mathbf{y}|)}{|\mathbf{x}-\mathbf{y}|}\, ds_{\mathbf{y}}\, ds_{\mathbf{x}} \\
&= 2\Delta t e^{-2\sigma t^n} \int_{T'}\int_{\tilde{P}} \frac{\partial_t f(\mathbf{y}, t^n-|\mathbf{x}-\mathbf{y}|)}{|\mathbf{x}-\mathbf{y}|}\, ds_{\mathbf{y}}\, ds_{\mathbf{x}} \\
&= 2\Delta t e^{-2\sigma t^n} \int_{T'}\int_{\tilde{P}} \sum_{T\in\mathcal{T}} \frac{\chi_T(\mathbf{x})\partial_t c_T(t^n-|\mathbf{x}-\mathbf{y}|)}{|\mathbf{x}-\mathbf{y}|}\, ds_{\mathbf{y}}\, ds_{\mathbf{x}} \\
&= 2\Delta t e^{-2\sigma t^n} \sum_{T\in\mathcal{T}} \int_{T'}\int_{\tilde{P}} \frac{\chi_T(\mathbf{x})\partial_t c_T(t^n-|\mathbf{x}-\mathbf{y}|)}{|\mathbf{x}-\mathbf{y}|}\, ds_{\mathbf{y}}\, ds_{\mathbf{x}} \\
&= 2\Delta t e^{-2\sigma t^n} \sum_{T\in\mathcal{T}} \int_{T'}\int_{T} \frac{\partial_t c_T(t^n-|\mathbf{x}-\mathbf{y}|)}{|\mathbf{x}-\mathbf{y}|}\, ds_{\mathbf{y}}\, ds_{\mathbf{x}} \\
&= 2\Delta t e^{-2\sigma t^n} \sum_{T\in\mathcal{T}\setminus T'} \int_{T'}\int_{T} \frac{\partial_t c_T(t^n-|\mathbf{x}-\mathbf{y}|)}{|\mathbf{x}-\mathbf{y}|}\, ds_{\mathbf{y}}\, ds_{\mathbf{x}} \\
&\quad + 2\Delta t e^{-2\sigma t^n} \int_{T'}\int_{T'} \frac{\partial_t c_{T'}(t^n-|\mathbf{x}-\mathbf{y}|)}{|\mathbf{x}-\mathbf{y}|}\, ds_{\mathbf{y}}\, ds_{\mathbf{x}}
\end{aligned}$$

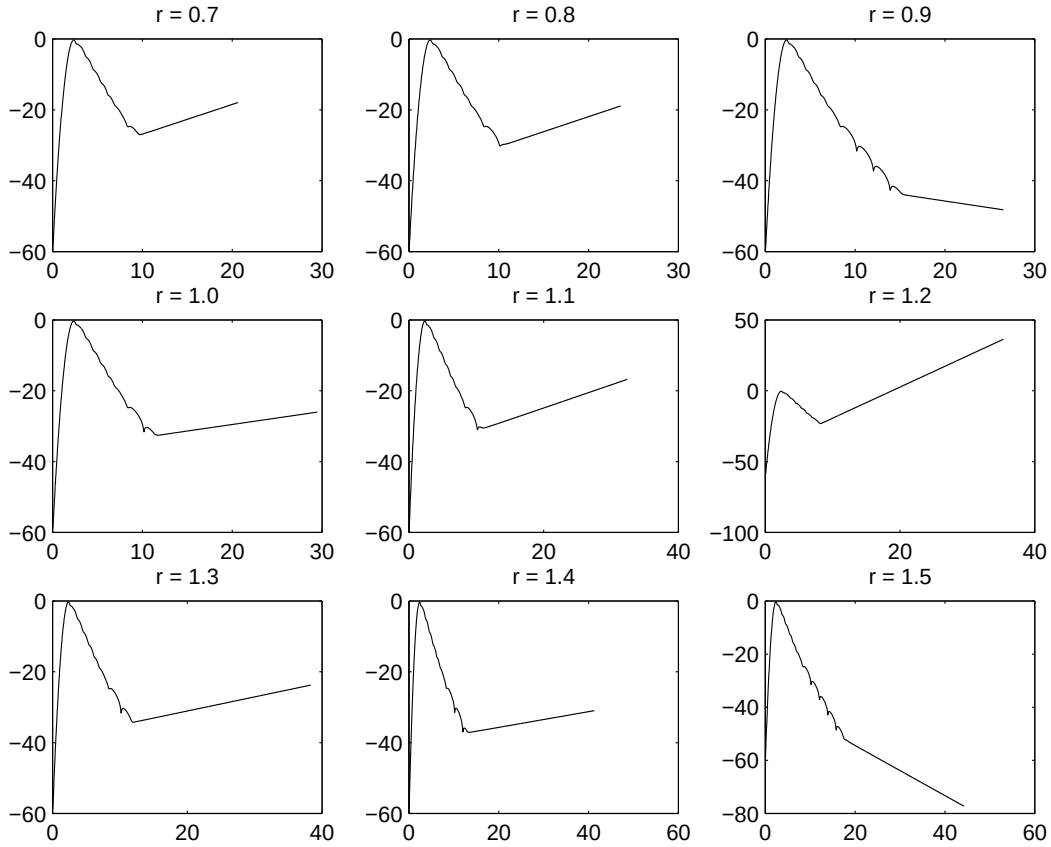

Figure 7: Logarithm of the L^2–norm of the numerical solution versus time for the collocation method for different meshratios r on a 16×16 mesh.

The integrals in the sum are approximated by the three–point Gauss rule. Let Φ_T be the affine–linear transformation mapping the triangle $T_{ref} = \text{conv}\,[(0,0),(1,0),(0,1)]$ to T. It is then

$$\begin{aligned}
\int_{T'}\int_{T} \frac{\partial_t c_T(t^n - |\mathbf{x}-\mathbf{y}|)}{|\mathbf{x}-\mathbf{y}|}\, ds_{\mathbf{y}}\, ds_{\mathbf{x}} &= \int_{T_{ref}}\int_{T_{ref}} \frac{\partial_t c_T(t^n - |\Phi_{T'}(\mathbf{x}) - \Phi_T(\mathbf{y})|)}{|\Phi_{T'}(\mathbf{x}) - \Phi_T(\mathbf{y})|} \text{gram}\,\Phi_T\, ds_{\mathbf{y}} \text{gram}\,\Phi_{T'}\, ds_{\mathbf{x}} \\
&\approx \sum_{\beta=1}^{3} \int_{T_{ref}} \omega_\beta \frac{\partial_t c_T(t^n - |\Phi_{T'}(\mathbf{x}) - \Phi_T(\xi_\beta)|)}{|\Phi_{T'}(\mathbf{x}) - \Phi_T(\xi_\beta)|} \text{gram}\,\Phi_T \text{gram}\,\Phi_{T'}\, ds_{\mathbf{x}} \\
&\approx \sum_{\alpha=1}^{3} \omega_\alpha \sum_{\beta=1}^{3} \omega_\beta \frac{\partial_t c_T(t^n - |\Phi_{T'}(\xi_\alpha) - \Phi_T(\xi_\beta)|)}{|\Phi_{T'}(\xi_\alpha) - \Phi_T(\xi_\beta)|} \text{gram}\,\Phi_T \text{gram}\,\Phi_{T'} \\
&= \sum_{\alpha,\beta=1}^{3} \omega_\alpha \omega_\beta \frac{\partial_t c_T(t^n - |\Phi_{T'}(\xi_\alpha) - \Phi_T(\xi_\beta)|)}{|\Phi_{T'}(\xi_\alpha) - \Phi_T(\xi_\beta)|} \text{gram}\,\Phi_T \text{gram}\,\Phi_{T'},
\end{aligned}$$

where $\xi_\alpha, \alpha = 1,...,3$ are the Gauss–points on T_{ref} and $\omega_\alpha, \alpha = 1,...,3$ the corresponding weights. The *selfpatch*–integral is

$$\int_{T'}\int_{T'} \frac{\partial_t c_{T'}(t^n - |\mathbf{x}-\mathbf{y}|)}{|\mathbf{x}-\mathbf{y}|}\, ds_{\mathbf{y}}\, ds_{\mathbf{x}} \approx \partial_t c_{T'}(t^n) \frac{\text{gram}\,\Phi_{T'}}{2} \int_{T'} \frac{1}{|\mathbf{x}_{T'} - \mathbf{y}|}\, ds_{\mathbf{y}}.$$

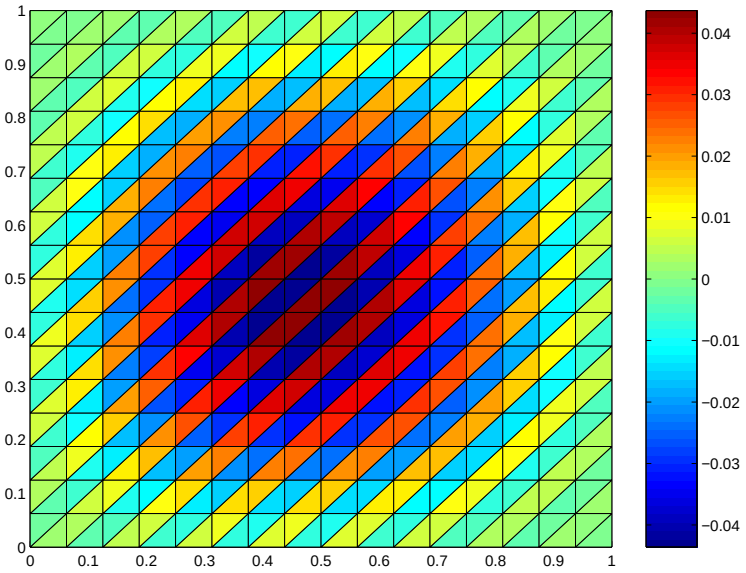

Figure 8: Unstable solution after 500 timesteps at a meshratio 0.6. Notice the regularity of the instability

For the linear form (18) one gets

$$\int_0^\infty e^{-2\sigma t} \int_{\tilde{P}} \chi_{T'}(\mathbf{x})\psi_n(t)\partial_t g(\mathbf{x},t)\, ds_{\mathbf{x}}\, dt \approx 2\Delta t e^{-2\sigma t^n} \operatorname{gram} \Phi_{T'} \sum_{\alpha=1}^{3} \omega_\alpha \partial_t g(\Phi_{T'}(\xi_\alpha), t^n).$$

After dividing by $\operatorname{gram} \Phi_{T'}$ and $2\Delta t e^{-2\sigma t^n}$ the above approximations result in the equation

$$C_{T',T'}\partial_t c_{T'}(t^n) = \sum_{\alpha=1}^{3} \omega_\alpha \partial_t g(\Phi_{T'}(\xi_\alpha), t^n) - \sum_{T\in\mathcal{T}\setminus T'} \sum_{\alpha,\beta=1}^{3} C_{T',T}^{\alpha,\beta} \partial_t c_T(t^n - |\Phi_{T'}(\xi_\alpha) - \Phi_T(\xi_\beta)|), \tag{23}$$

where

$$\begin{aligned} C_{T',T'} &= \frac{1}{2}\int_{T'} \frac{1}{|\mathbf{x}_{T'} - \mathbf{y}|}\, ds_{\mathbf{y}}, \\ C_{T',T}^{\alpha,\beta} &= \omega_\alpha\omega_\beta \frac{\operatorname{gram}\Phi_T}{|\Phi_{T'}(\xi_\alpha) - \Phi_T(\xi_\beta)|}. \end{aligned}$$

Performing an integration in time of (23) and using $c_{T'}(0) = g(\cdot, 0) = 0$ gives

$$C_{T',T'}c_{T'}(t^n) = \sum_{\alpha=1}^{3} \omega_\alpha g(\Phi_{T'}(\xi_\alpha), t^n) - \sum_{T\in\mathcal{T}\setminus T'} \sum_{\alpha,\beta=1}^{3} C_{T',T}^{\alpha,\beta} c_T(t^n - |\Phi_{T'}(\xi_\alpha) - \Phi_T(\xi_\beta)|). \tag{24}$$

This step can be done, since, as will be seen later, the right–hand–side g will always be identically zero at $t = 0$ and the solution u too. The terms $c_T(t^n - |\Phi_{T'}(\xi_\alpha) - \Phi_T(\xi_\beta)|)$ can again be interpolated between the integer multiples of the time–step size Δt, which gives

$$c_T(t^n - |\Phi_{T'}(\xi_\alpha) - \Phi_T(\xi_\beta)|) = (1 - \epsilon_{T',T}^{\alpha,\beta}) c_T((n - m_{T',T}^{\alpha,\beta})\Delta t) + \epsilon_{T',T}^{\alpha,\beta} c_T((n - m_{T',T}^{\alpha,\beta} - 1)\Delta t),$$

where

$$m_{T',T}^{\alpha,\beta} = \lfloor |\Phi_{T'}(\xi_\alpha) - \Phi_T(\xi_\beta)|/\Delta t \rfloor \quad \text{and} \quad \epsilon_{T',T}^{\alpha,\beta} = |\Phi_{T'}(\xi_\alpha) - \Phi_T(\xi_\beta)|/\Delta t - m_{T',T}^{\alpha,\beta}.$$

Substituting this into (24) gives

$$\begin{aligned} C_{T',T'}u^n_{T'} &= \sum_{\alpha=1}^{3}\omega_\alpha g(\Phi_{T'}(\xi_\alpha), n\Delta t) \\ &\quad - \sum_{T\in\mathcal{T}\setminus T'}\sum_{\alpha,\beta=1}^{3} C^{\alpha,\beta}_{T',T}((1-\epsilon^{\alpha,\beta}_{T',T})u_T^{(n-m^{\alpha,\beta}_{T',T})} + \epsilon^{\alpha,\beta}_{T',T}u_T^{(n-m^{\alpha,\beta}_{T',T}-1)}). \end{aligned}$$

Equation (24) can now be written in matrix notation, i.e. testing against all basis functions ψ_T simultaneously. The discrete solution $U \in V_{\mathcal{T},\Delta t}$ satisfies, using the initial condition $\mathbf{U}^0 = \mathbf{0}$, the equation

$$Q^0\mathbf{U}^n = \mathbf{b}^n - \sum_{m=1}^{n-1} Q^m\mathbf{U}^{n-m},$$

where $\mathbf{U}^i$, $\mathbf{b}^i$ are the vectors with components $u^i_{T'}$ and $\sum_{\alpha=1}^{3}\omega_\alpha g(\Phi_{T'}(\xi_\alpha), i\Delta t)$ respectively. The matrices Q^m are given by

$$Q^m(j,k) = \sum_{m^{\alpha,\beta}_{T_j,T_k}=m} C^{\alpha,\beta}_{T_j,T_k}(1-\epsilon^{\alpha,\beta}_{T_j,T_k}) + \sum_{m^{\alpha,\beta}_{T_j,T_k}=m-1} C^{\alpha,\beta}_{T_j,T_k}\epsilon^{\alpha,\beta}_{T_j,T_k}, \qquad \text{if } m \neq 0,$$

$$Q^0(j,k) = \begin{cases} C_{T_j,T_j}, & \text{if } j = k, \\ \sum_{m^{\alpha,\beta}_{T_j,T_k}=0} C^{\alpha,\beta}_{T_j,T_k}(1-\epsilon^{\alpha,\beta}_{T_j,T_k}), & \text{else.} \end{cases}$$

Here, the matrix Q^0 is diagonal, if the time step size Δt divided by the minimal distance between the midpoint of a triangle and a Gauss point of another triangle is less than one. For halfed squares of size h this condition becomes $r < 1/2$, where r is defined as in the previous section. Figures 9 and 11 show numerical results for the example from section 3.1. For computational reasons h is chosen to be $1/8$, and all tested mesh ratios gave stable solutions. For the low mesh ratios the L^2–norm of the numerical solution reaches its maximum later than it should, i.e. the solution is wrong. This phenomenon is due to the big difference between $1/r$ and the speed of light, which is here nondimensionalised to unity. In practice this means, that some time–levels are left out in calculating a specific value. To obtain correct solutions, the mesh ratio should thus be chosen close to one. Figure 10 shows the stable solution after 500 time steps for $r = 0.6$ on the 16×16 mesh.

Remark. The integration step in the discretization improves the stabilty of the algorithm. Numerical examples for the scheme obtained by leaving out this step were unstable.

3.3 Calculating the Selfpatch

In the presented algorithms for solving the retarded potential integral equation, integrals of the form

$$\int_T \frac{1}{|\mathbf{x}-\mathbf{x}_T|}\, ds_{\mathbf{x}},$$

where $\mathbf{x}_T$ denotes the midpoint of T, have to be solved. This can be done either analytically or numerically.

3.3.1 Analytical Way

For simplicity, consider the triangle T_{ref}. The triangle can be moved so that the midpoint $\mathbf{x}_{T_{ref}}$ is equal to $(0,0)$. The triangle is divided into six triangles as shown in figure 12. It is then

$$\begin{aligned} \int_{T_{ref}} \frac{1}{|\mathbf{x}-\mathbf{x}_{T_{ref}}|}\, d\mathbf{x} &= \left(\int_{T_I+T_{II}+T_{III}+T_{I'}+T_{II'}+T_{III'}} \frac{1}{|\mathbf{x}|}\, d\mathbf{x}\right) \\ &= 2\left(\int_0^{\pi/4}\int_0^{\frac{1}{3\cos\phi}} \frac{1}{r}\, r\, dr\, d\phi \right. \end{aligned}$$

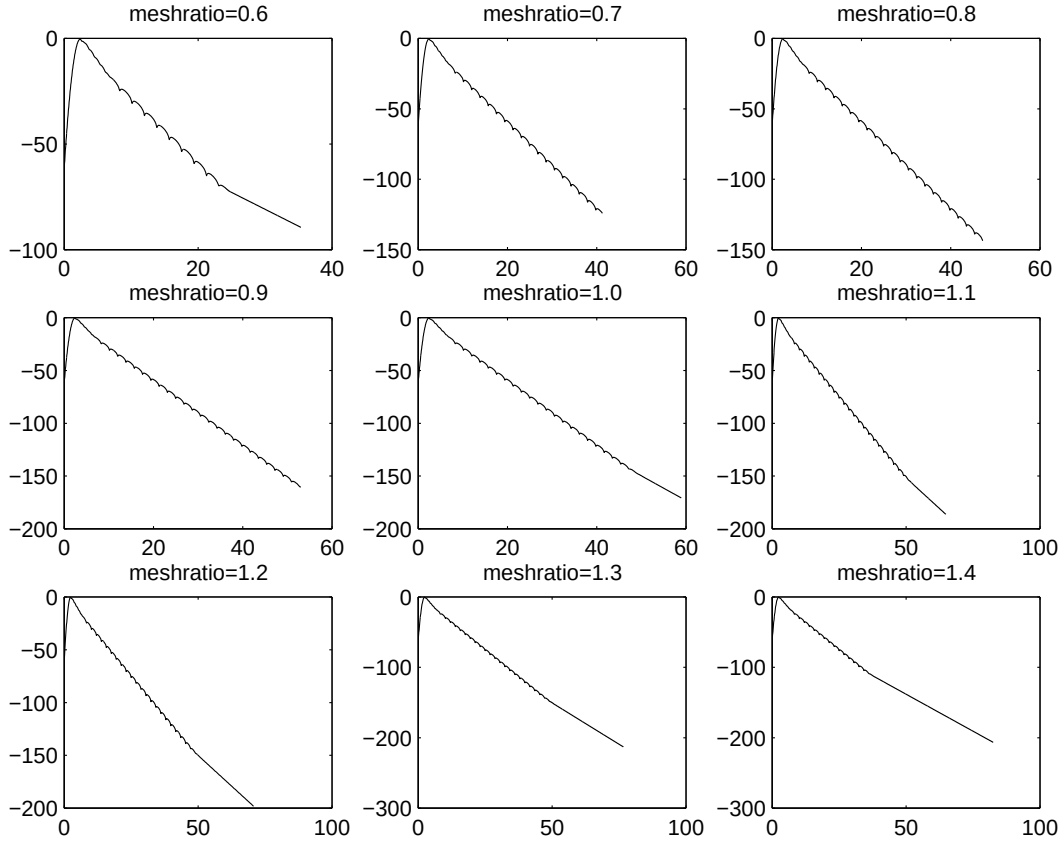

Figure 9: Logarithm of the L^2–norm of the numerical solution versus time for the Galerkin scheme

$$
\begin{aligned}
&+ \int_0^{\arccos(1/\sqrt{5})} \int_0^{\frac{1}{3\cos\phi}} \frac{1}{r} r \, dr \, d\phi \\
&+ \int_0^{3\pi/4-\arccos(1/\sqrt{5})} \int_0^{\frac{1}{3\sqrt{2}\cos\phi}} \frac{1}{r} r \, dr \, d\phi \Bigg) \\
= \;& 2 \left(\int_0^{\pi/4} \frac{1}{3\cos\phi} \, d\phi + \int_0^{\arccos(1/\sqrt{5})} \frac{1}{3\cos\phi} \, d\phi \right. \\
&\left. + \int_0^{3\pi/4-\arccos(1/\sqrt{5})} \frac{1}{3\sqrt{2}\cos\phi} \, d\phi \right) \\
= \;& \frac{2}{3} \left(\left[\ln \left| \tan \frac{\pi}{2} + \frac{\phi}{2} \right| \right]_0^{\pi/4} + \left[\ln \left| \tan \frac{\pi}{2} + \frac{\phi}{2} \right| \right]_0^{\arccos(1/\sqrt{5})} \right. \\
&\left. + \frac{1}{\sqrt{2}} \left[\ln \left| \tan \frac{\pi}{2} + \frac{\phi}{2} \right| \right]_0^{3\pi/4-\arccos(1/\sqrt{5})} \right) \\
= \;& \frac{2}{3} \left(\ln \left| \frac{1+\tan\alpha/2}{1-\tan\alpha/2} \right| + \ln \left| \frac{1+\tan\beta/2}{1-\tan\beta/2} \right| + \frac{1}{\sqrt{2}} \ln \left| \frac{1+\tan\gamma/2}{1-\tan\gamma/2} \right| \right) \\
= \;& 2.4072,
\end{aligned}
$$

where $\alpha = \pi/4$, $\beta = \arccos(1/\sqrt{5})$ and $\gamma = 3\pi/4 - \arccos(1/\sqrt{5})$. If the side of the triangle is h, the transformation formula gives the value $2.4072h$.

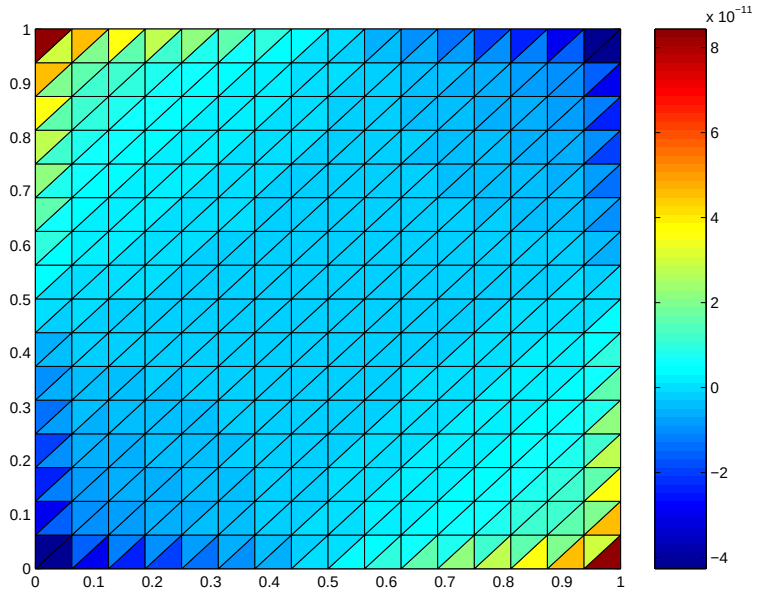

Figure 10: Stable solution after 500 time steps for the mesh ratio $r = 0.6$

3.3.2 Quadrature–Formulae for singular Integrands on Triangles

Let f be an integrable function on $T_{ref,2} := \text{conv}\,[(0,0),(1,0),(1,1)]$. It is

$$\begin{aligned}\int_{T_{ref,2}} f(x,y)\,d(x,y) &= \int_0^1 \int_0^x f(x,y)\,dy\,dx \\ &= \int_0^1 \int_0^1 f(x,xs)x\,ds\,dx.\end{aligned}$$

This transformation is due to Duffy, and can be found in [Duf]. If the integrand f has a singularity at the origin and $f(x,y) = g(x,y)\cdot(x^2+y^2)^{(-\alpha/2)}$ for a function $g \in C(\overline{T_{ref,2}})$ and a positive constant $\alpha \in \mathbb{R}$, then it is

$$f(x,xs)x = g(x,xs)x^{1-\alpha}(1+s^2)^{-\alpha/2}.$$

This means that for $\alpha \leq 1$ the mapping $(x,s) \mapsto f(x,xs)x$ is nonsingular. Any well–known quadrature-formula for the unit square can now be applied to the integral and gives one for the triangle $T_{ref,2}$. The table below shows how the midpoint– and the four point Gauss–rule transform.

Approximation–type	Quadrature–points on $[0,1]^2$	Transformed points on $T_{ref,2}$
Midpoint rule	$\xi = (1/2, 1/2)$ $\omega = 1$	$\eta = (1/2, 1/4)$ $\theta = 1/2$
Gauss 4–point rule	$\xi_1 = (\frac{1}{2} - \frac{1}{\sqrt{12}}, \frac{1}{2} - \frac{1}{\sqrt{12}})$ $\xi_2 = (\frac{1}{2} + \frac{1}{\sqrt{12}}, \frac{1}{2} - \frac{1}{\sqrt{12}})$ $\xi_3 = (\frac{1}{2} - \frac{1}{\sqrt{12}}, \frac{1}{2} + \frac{1}{\sqrt{12}})$ $\xi_4 = (\frac{1}{2} + \frac{1}{\sqrt{12}}, \frac{1}{2} + \frac{1}{\sqrt{12}})$ $\omega_i = 1/4$	$\eta_1 = (\frac{1}{2} - \frac{1}{\sqrt{12}}, \frac{1}{3} - \frac{1}{2\sqrt{3}})$ $\eta_2 = (\frac{1}{2} + \frac{1}{\sqrt{12}}, \frac{1}{6})$ $\eta_3 = (\frac{1}{2} - \frac{1}{\sqrt{12}}, \frac{1}{6})$ $\eta_4 = (\frac{1}{2} + \frac{1}{\sqrt{12}}, \frac{1}{3} + \frac{1}{2\sqrt{3}})$ $\theta_1 = \frac{1}{4}(\frac{1}{2} - \frac{1}{\sqrt{12}})$ $\theta_2 = \frac{1}{4}(\frac{1}{2} + \frac{1}{\sqrt{12}})$ $\theta_3 = \frac{1}{4}(\frac{1}{2} - \frac{1}{\sqrt{12}})$ $\theta_4 = \frac{1}{4}(\frac{1}{2} + \frac{1}{\sqrt{12}})$

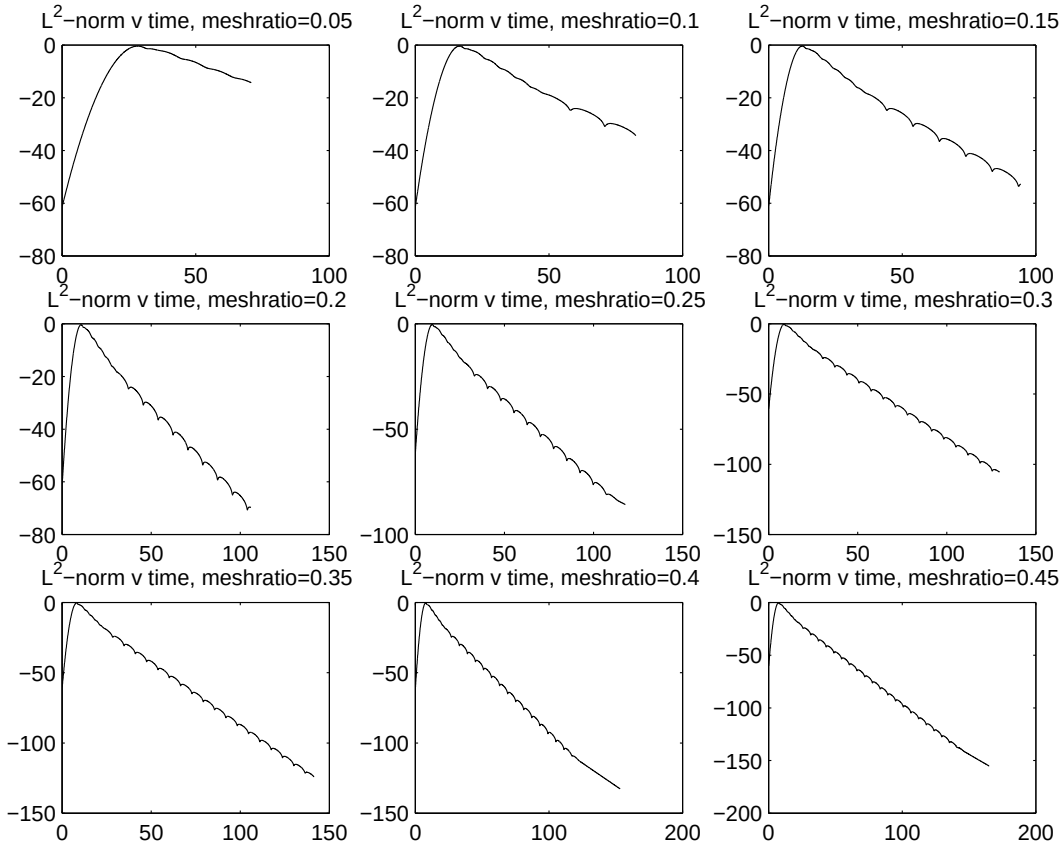

Figure 11: Logarithm of the L^2–norm of the numerical solution versus time for the Galerkin scheme at small meshratios

To evaluate integrals which have a singularity at the midpoint, for example

$$\int_{T_{ref}} \frac{1}{|\mathbf{x} - \mathbf{x}_{T_{ref}}|}\, ds_{\mathbf{x}},$$

T_{ref} is divided into three subtriangles as shown in figure 13. Each of them contains a singularity at one vertex. By affine–linear transformations the subtriangles are mapped to $T_{ref,2}$ such that the singularity is mapped to the origin. In this way, quadrature formulae for integrating functions with a singularity of degree $\alpha \leq 1$ over the reference triangle can be obtained. The affine–linear mappings are

$$\begin{aligned}
&\Phi_I : T_{ref,2} \to T_I, \quad (\xi_1, \xi_2) \mapsto ((1-\xi_1)/3 + \xi_2, (1-\xi_1)/3) \\
&\Phi_{II} : T_{ref,2} \to T_{II}, \quad (\xi_1, \xi_2) \mapsto ((1-\xi_1)/3 + (\xi_1 - \xi_2), (1-\xi_1)/3 + \xi_2) \\
&\Phi_{III} : T_{ref,2} \to T_{III}, \quad (\xi_1, \xi_2) \mapsto ((1-\xi_1)/3, (\xi_1 - \xi_2)).
\end{aligned}$$

The midpoint rule gives the three quadrature points $(\frac{5}{12}, \frac{2}{12})$, $(\frac{5}{12}, \frac{5}{12})$ and $(\frac{2}{12}, \frac{5}{12})$ with weights $\frac{1}{6}$, i.e.

$$\int_{T_{ref}} f(\mathbf{x})\, d\mathbf{x} \approx \frac{1}{6}\left(f\left(\frac{5}{12}, \frac{2}{12}\right) + f\left(\frac{5}{12}, \frac{5}{12}\right) + f\left(\frac{2}{12}, \frac{5}{12}\right)\right),$$

while the four–point rule gives the twelve points

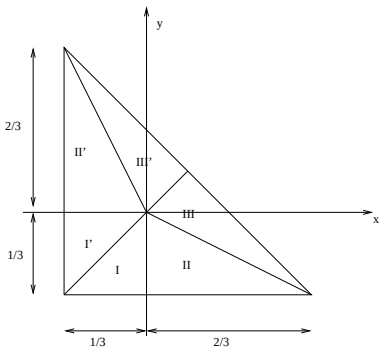

Figure 12: Division of the triangle

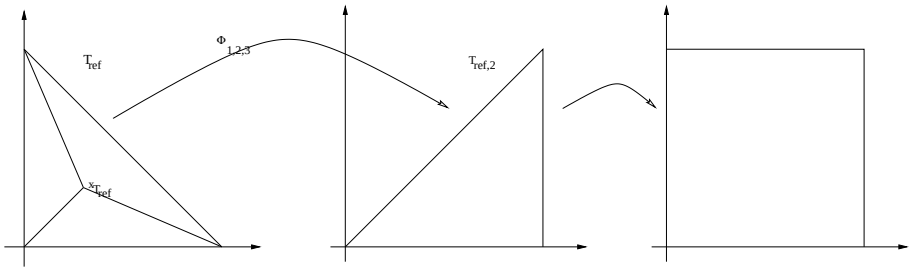

Figure 13: Division of the triangle and mapping to the unit square

i	1	2	3	4	5	6
ξ_i^1	$\frac{1}{2}-\frac{1}{3\sqrt{3}}$	$\frac{1}{3}-\frac{1}{6\sqrt{3}}$	$\frac{1}{3}+\frac{1}{6\sqrt{3}}$	$\frac{1}{2}+\frac{1}{3\sqrt{3}}$	$\frac{1}{3}+\frac{1}{6\sqrt{3}}$	$\frac{1}{2}+\frac{1}{3\sqrt{3}}$
ξ_i^2	$\frac{1}{6}+\frac{1}{6\sqrt{3}}$	$\frac{1}{6}-\frac{1}{6\sqrt{3}}$	$\frac{1}{6}+\frac{1}{6\sqrt{3}}$	$\frac{1}{6}-\frac{1}{6\sqrt{3}}$	$\frac{1}{2}-\frac{1}{3\sqrt{3}}$	$\frac{1}{3}-\frac{1}{6\sqrt{3}}$
ω_i	$\frac{1}{12}\left(\frac{1}{2}-\frac{1}{2\sqrt{3}}\right)$	$\frac{1}{12}\left(\frac{1}{2}+\frac{1}{2\sqrt{3}}\right)$	$\frac{1}{12}\left(\frac{1}{2}-\frac{1}{2\sqrt{3}}\right)$	$\frac{1}{12}\left(\frac{1}{2}+\frac{1}{2\sqrt{3}}\right)$	$\frac{1}{12}\left(\frac{1}{2}-\frac{1}{2\sqrt{3}}\right)$	$\frac{1}{12}\left(\frac{1}{2}+\frac{1}{2\sqrt{3}}\right)$
i	7	8	9	10	11	12
ξ_i^1	$\frac{1}{2}-\frac{1}{3\sqrt{3}}$	$\frac{1}{3}-\frac{1}{6\sqrt{3}}$	$\frac{1}{6}+\frac{1}{6\sqrt{3}}$	$\frac{1}{6}-\frac{1}{6\sqrt{3}}$	$\frac{1}{6}+\frac{1}{6\sqrt{3}}$	$\frac{1}{6}-\frac{1}{6\sqrt{3}}$
ξ_i^2	$\frac{1}{3}+\frac{1}{6\sqrt{3}}$	$\frac{1}{2}+\frac{1}{3\sqrt{3}}$	$\frac{1}{3}+\frac{1}{6\sqrt{3}}$	$\frac{1}{2}+\frac{1}{3\sqrt{3}}$	$\frac{1}{2}-\frac{1}{3\sqrt{3}}$	$\frac{1}{3}-\frac{1}{6\sqrt{3}}$
ω_i	$\frac{1}{12}\left(\frac{1}{2}-\frac{1}{2\sqrt{3}}\right)$	$\frac{1}{12}\left(\frac{1}{2}+\frac{1}{2\sqrt{3}}\right)$	$\frac{1}{12}\left(\frac{1}{2}-\frac{1}{2\sqrt{3}}\right)$	$\frac{1}{12}\left(\frac{1}{2}+\frac{1}{2\sqrt{3}}\right)$	$\frac{1}{12}\left(\frac{1}{2}-\frac{1}{2\sqrt{3}}\right)$	$\frac{1}{12}\left(\frac{1}{2}+\frac{1}{2\sqrt{3}}\right)$

For the integral $\int_{T_{ref}} \frac{1}{|\mathbf{x}_{T_{ref}}-\mathbf{x}|}\, ds_{\mathbf{x}}$ one gets

3 points	12 points	standard Gauss 3–point	analytically
3.20306	2.23686	1.60153	2.4072

Thus at least a 12–point rule should be used in the presented schemes.

3.4 A Numerical Stability Test for Time–Stepping Algorithms

Bamberger and Duong state a theorem for the stability of the Galerkin scheme.

Theorem 6 *The Galerkin scheme*
Find $\rho_{\Delta t,\mathcal{T}} \in V_{\Delta t,\mathcal{T}}$ such that

$$a(\rho_{\Delta t,\mathcal{T}}, \psi_{\Delta t,\mathcal{T}}) = b(\psi_{\Delta t,\mathcal{T}}) \qquad (\psi_{\Delta t,\mathcal{T}} \in V_{\Delta t,\mathcal{T}})$$

is stable in the sense that there exists a constant C independent of h and Δt such that

$$|\rho_{\Delta t,\mathcal{T}}|_{\sigma,-1/2,-1/2} \leq C$$

for $h, \Delta t \to 0$, where h is the maximal diameter of triangles in $\mathcal{T}$.

In this sense of stability, the solution may still grow in time since the norm $|\cdot|_{\sigma,-1/2,-1/2}$ involves an exponentially decaying term.
Problems in discretizing the integral equation were illustrated in the previous sections and numerical experiments show that stability is dependent on the approximations of for example the selfpatch integral. In order to obtain a stability criterion for the discretized schemes, the retarded potential integral equation is considered on an infinite flat plate that is uniformly covered with triangles of side h as shown in figure 14. The schemes resulting from the direct approach as in section 3.1 or from the Galerkin method as in section 3.2 need to be expressed in shift operators. This form of the algorithm will allow to calculate amplification factors which will indicate stability. It seems likely, that if the algorithm is stable on the infinite plate, it will also be stable for finite plates though this will depend on the special geometry. It is reasonable to consider the scheme on a flat plate since one cannot expect that the algorithm will be stable for a curved surface if it is not on a flat plate.

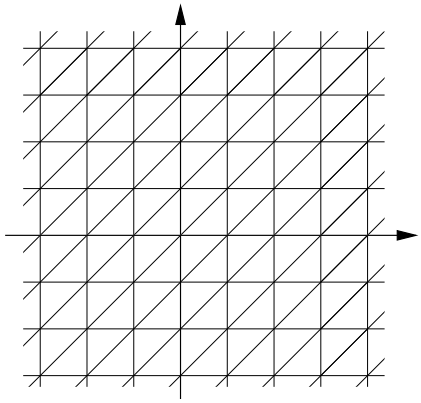

Figure 14: Infinite triangulation of $\mathbb{R}^2$

3.4.1 Preliminaries

Let $\mathcal{T}$ denote the uniform triangulation of $\mathbb{R}^2$ with triangles of side h shown in figure 14. A function f that is constant on every triangle $T \in \mathcal{T}$ is identified with a mesh function $f^* : \mathbb{Z}^2 \to \mathbb{R}^2$ that is defined by

$$f^*_{n,m} = (\alpha, \beta), \quad \text{if} \quad f|_{T^{upper}_{n,m}} = \alpha \quad \text{and} \quad f|_{T^{lower}_{n,m}} = \beta,$$

where

$$\begin{aligned} T^{upper}_{n,m} &= \text{conv}\,[(nh, mh), ((n+1)h, mh), ((n+1)h, (m+1)h)] \qquad \text{and} \\ T^{lower}_{n,m} &= \text{conv}\,[(nh, mh), ((n+1)h, (m+1)h), (nh, (m+1)h)]. \end{aligned}$$

A mesh function f is an element of $L^2(\mathcal{T})$ if

$$\|f\|^2_{L^2(\mathcal{T})} := h^2 \sum_{(n,m)\in\mathbb{Z}^2} |f_{n,m}|^2 < \infty$$

and $f \in L^1(\mathcal{T})$ if

$$\|f\|_{L^1(\mathcal{T})} := h^2 \sum_{(n,m)\in\mathbb{Z}^2} |f_{n,m}| < \infty.$$

The *discrete fourier–transformed* (DFT) $\tilde{f}$ of a function $f \in L^2(\mathcal{T}) \cap L^1(\mathcal{T})$ is defined as

$$\tilde{f}(\omega) = h^2 \sum_{(n,m)\in\mathbb{Z}^2} e^{-i\omega\cdot(n,m)h} f_{n,m}, \quad \omega \in [0, 2\pi/h]^2$$

and can be extended to the whole $L^2(\mathcal{T})$. The inverse of the DFT is given by

$$f_{n,m} = \frac{1}{4\pi^2} \int_{[0,2\pi/h]^2} \tilde{f} e^{i\omega\cdot(n,m)}\, d\omega, \qquad (n,m) \in \mathbb{Z}^2.$$

As in the continuous situation, the DFT is an isometric isomorphism from $L^2(\mathcal{T})$ to $L^2([0,2\pi/h]^2)$. The shift–operators S_x and S_y on $L^2(\mathcal{T})$ defined by

$$(S_x f)_{n,m} = f_{n+1,m}, \quad (S_y f)_{n,m} = f_{n,m+1}$$

transform as follows:

$$\begin{aligned}
(S_x^j S_y^k f)\tilde{}\,(\omega) &= h^2 \sum_{(n,m)\in\mathbb{Z}^2} e^{-i\omega\cdot(n,m)h} (S_x^j S_y^k f)_{n,m} \\
&= h^2 \sum_{(n,m)\in\mathbb{Z}^2} e^{-i\omega\cdot(n,m)h} f_{n+j,m+k} \\
&= h^2 \sum_{(n,m)\in\mathbb{Z}^2} e^{-i\omega\cdot((n+j)-j,(m+k)-k)h} f_{n+j,m+k} \\
&= h^2 \sum_{(r,s)\in\mathbb{Z}^2} e^{-i\omega\cdot(r-j,s-k)h} f_{r,s} \\
&= e^{i\omega\cdot(j,k)h} h^2 \sum_{(r,s)\in\mathbb{Z}^2} e^{-i\omega\cdot(r,s)h} f_{r,s} \\
&= e^{i\omega\cdot(j,k)h} \tilde{f}(\omega), \qquad (j,k) \in \mathbb{Z}^2.
\end{aligned}$$

3.4.2 Infinite Plate Algorithm in Shift–Operator Notation

As for a finite plate, discretizing the retarded potential integral equation according to the direct approach results in the scheme

$$\begin{aligned}
&C_{T^{lower}_{j,k},T^{lower}_{j,k}} U^n_{T^{lower}_{j,k}} = g(x_{T^{lower}_{j,k}}, t^n) \\
&- \sum_{(l,m)\in\mathbb{Z}^2\setminus(j,k)} C_{T^{lower}_{l,m},T^{lower}_{j,k}} \left((1-\epsilon_{T^{lower}_{l,m},T^{lower}_{j,k}}) U_{T^{lower}_{l,m}}^{n-m_{T^{lower}_{l,m},T^{lower}_{j,k}}} + \epsilon_{T^{lower}_{l,m},T^{lower}_{j,k}} U_{T^{lower}_{l,m}}^{n-m_{T^{lower}_{l,m},T^{lower}_{j,k}}-1}\right) \\
&- \sum_{(l,m)\in\mathbb{Z}^2} C_{T^{upper}_{l,m},T^{lower}_{j,k}} \left((1-\epsilon_{T^{upper}_{l,m},T^{lower}_{j,k}}) U_{T^{upper}_{l,m}}^{n-m_{T^{upper}_{l,m},T^{lower}_{j,k}}} + \epsilon_{T^{upper}_{l,m},T^{lower}_{j,k}} U_{T^{upper}_{l,m}}^{n-m_{T^{upper}_{l,m},T^{lower}_{j,k}}-1}\right),
\end{aligned}$$

for lower triangles and

$$\begin{aligned}
&C_{T^{upper}_{j,k},T^{upper}_{j,k}} U^n_{T^{upper}_{j,k}} = g(x_{T^{upper}_{j,k}}, t^n) \\
&- \sum_{(l,m)\in\mathbb{Z}^2} C_{T^{lower}_{l,m},T^{upper}_{j,k}} \left((1-\epsilon_{T^{lower}_{l,m},T^{upper}_{j,k}}) U_{T^{lower}_{l,m}}^{n-m_{T^{lower}_{l,m},T^{upper}_{j,k}}} + \epsilon_{T^{lower}_{l,m},T^{upper}_{j,k}} U_{T^{lower}_{l,m}}^{n-m_{T^{lower}_{l,m},T^{upper}_{j,k}}-1}\right) \\
&- \sum_{(l,m)\in\mathbb{Z}^2\setminus(j,k)} C_{T^{upper}_{l,m},T^{upper}_{j,k}} \left((1-\epsilon_{T^{upper}_{l,m},T^{upper}_{j,k}}) U_{T^{upper}_{l,m}}^{n-m_{T^{upper}_{l,m},T^{upper}_{j,k}}} + \epsilon_{T^{upper}_{l,m},T^{upper}_{j,k}} U_{T^{upper}_{l,m}}^{n-m_{T^{upper}_{l,m},T^{upper}_{j,k}}-1}\right)
\end{aligned}$$

for upper triangles. Setting $\mathbf{U}^n_{j,k} = (U|^n_{T^{lower}_{j,k}}, U|^n_{T^{upper}_{j,k}})$ the equations can be written as

$$\mathcal{Q}^0 \mathbf{U}^n_{j,k} = \mathbf{g}^n - \sum_{m=1}^{n} \mathcal{Q}^m \mathbf{U}^{n-m}_{j,k} \tag{25}$$

where the $\mathcal{Q}^j$'s are 2×2-matrices whose entries are rational polynomials in the shift–operators S_x and S_y. In contrast to the scheme given in section 3.1 the initial data $\mathbf{U}^0_{j,k}$ is included. Stability criteria should not depend on the forcing function g and thus in the following g is taken to be identically zero but non–zero data at time $t = 0$ and zero–data for times $t < 0$ are assumed. The matrices $\mathcal{Q}^j$ can be calculated as follows: Without loss of generality, take $(j,k) = (0,0)$ and let $(r,s) \in \mathbb{Z}^2$. Then in calculating $\mathbf{U}^n_{j,k}$, the triangle $T^{upper}_{r,s}$ contributes the amounts

$$(1 - \epsilon_{T^{upper}_{r,s},T^{upper}_{0,0}}) C_{T^{upper}_{r,s},T^{upper}_{0,0}} S_x^r S_y^s \quad \text{to} \quad \mathcal{Q}^{m_{T^{upper}_{r,s},T^{upper}_{0,0}}}(1,1) \text{ and}$$

$$\epsilon_{T^{upper}_{r,s},T^{upper}_{0,0}} C_{T^{upper}_{r,s},T^{upper}_{0,0}} S_x^r S_y^s \quad \text{to} \quad \mathcal{Q}^{m_{T^{upper}_{r,s},T^{upper}_{0,0}}+1}(1,1),$$

where the values $\epsilon_{T^{upper}_{r,s},T^{upper}_{0,0}}$, $m_{T^{upper}_{r,s},T^{upper}_{0,0}}$ and $\epsilon_{T^{upper}_{r,s},T^{upper}_{0,0}}$ are the same as in section 3.1. The contribution from the lower triangle is calculated similarly and adds to

$$\mathcal{Q}^{m_{T^{lower}_{r,s},T^{upper}_{0,0}}}(1,2) \text{ and } \mathcal{Q}^{m_{T^{lower}_{r,s},T^{upper}_{0,0}}+1}(1,2).$$

Analogously, the rational polynomials $\mathcal{Q}^l(2,1)$ and $\mathcal{Q}^l(2,2)$ are calculated.
If the retarded potential integral equation is discretized according to the Galerkin-Ansatz, the same ideas lead to a scheme like (25).

3.4.3 Fourier–Transformed Algorithm

Carrying out a Fourier–transformation of the scheme (25)

$$\mathcal{Q}^0 \mathbf{U}^n_{j,k} = \sum_{m=1}^{n} \mathcal{Q}^m \mathbf{U}^{n-m}_{j,k} = \sum_{m=0}^{n-1} \mathcal{Q}^{n-m} \mathbf{U}^m_{j,k}$$

gives

$$q_0 \tilde{\mathbf{U}}^n = \sum_{m=0}^{n-1} q_{n-m} \tilde{\mathbf{U}}^m, \tag{26}$$

where $q_j = Q^j(e^{i\omega_1 h}, e^{i\omega_2 h})$, if $\mathcal{Q}^j = Q^j(S_x, S_y)$. Setting $p_0 = \begin{pmatrix} 1 & 0 \\ 0 & 1 \end{pmatrix}$ and $p_n = -q_0^{-1} \sum_{m=0}^{n-1} q_{n-m} p_m$ for $n \geq 1$, equation (26) can be written as

$$\tilde{\mathbf{U}}^n = p_n \tilde{\mathbf{U}}^0.$$

Davies gives in [Da2] the following definition of stability and proves a stability criterion for the infinite plate algorithm.

Definition 6 *The scheme (25) is called L^2–stable, if there exist constants A and C independent of $r = \Delta t/h$ and n such that for any initial mesh function U^0, solutions of (25) satisfy*

$$\|U^n\|_2 \leq C e^{An\Delta t} \|U^0\|_2.$$

Theorem 7 *The scheme (25) is L^2–stable if there exists a constant C such that*

$$\|p_n\|_\infty < C$$

for all n, with $\|p_n\|_\infty = \max\{|p_n(\omega)|, \omega \in [0, 2\pi/h]^2\}$.

Remark. The factors p_n are independent of the particular mesh–size h but depend on the meshratio $r = \Delta t/h$.
Figure 16 shows how the amplification factors p^D_n, arising from the direct discretization, grow exponentially with n at a frequency $(0, \pi/2h)$ while at the same frequency the amplification factors p^G_n for the Galerkin–scheme are bounded. In figure 17 plots of $p^D_{100}(\omega)$ for different meshratios indicate which frequencies are responsable for the instability. These frequencies are almost the same for $r = 0.6$ and $r = 1.2$. The plots of the maximum norm $\|p^G_n\|_{\infty,[0,2\pi/h]^2}$ in figure 18 suggest that the scheme due to the Galerkin–discretization is stable for all meshratios. These results are confirmed by several examples for the nonhomogeneous problem. Another stability–test for algorithms like the considered ones can be derived from the Z–transform, which simplifies the convolution sum. This stability–test seems to be sharper and was not in agreement with the examples from section 3.1 and 3.2 (see [PeSi]).

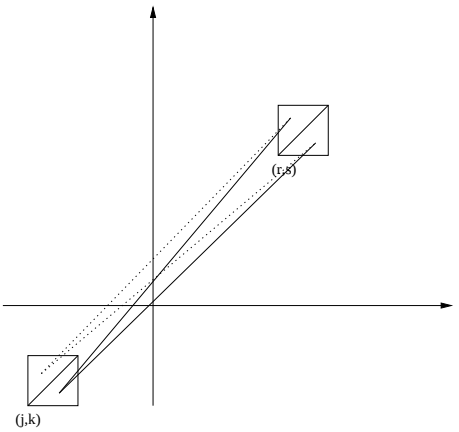

Figure 15: Influence of the triangle with left lower corner (r, s) on the triangle (j, k)

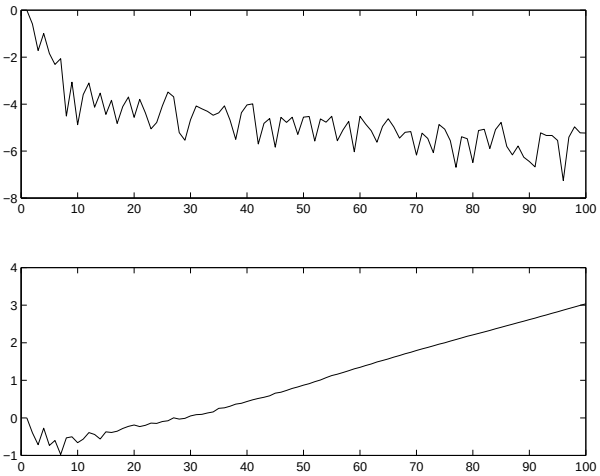

Figure 16: Comparison of the amplification factors p_n^G and p_n^D at a frequency $\omega = (0, \pi/2h)$ for $r = 1.2$

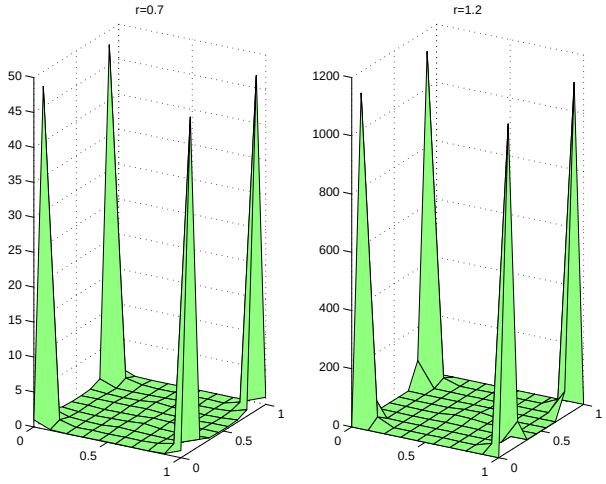

Figure 17: Amplification factors plotted against frequency for meshratio $r = 0.7$ and $n = 80$ (left) and $r = 1.2$ and $n = 50$ (right)

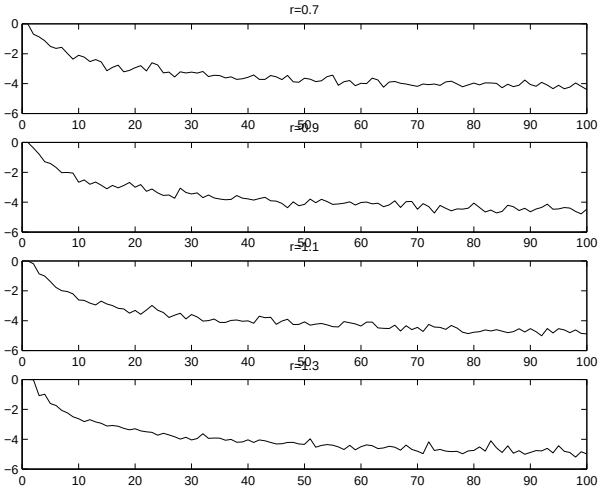

Figure 18: Logarithm of $\|p_n^G\|_\infty$, $n \in [1, 100]$

3.5 Other Approximations of the Selfpatch–Integral

The treatment of the self–patch integral in the given algorithms seems to be a bit unsatisfying. The quadrature formulae from section 3.3 can be applied directly to the integral

$$\int_T \int_T \frac{\partial_t c_T(t^n - |\mathbf{x} - \mathbf{y}|)}{|\mathbf{x} - \mathbf{y}|}\, ds_{\mathbf{y}}\, ds_{\mathbf{x}}$$

instead of taking the time–dependent function $\partial_t c_T$ to be constant on the set $\{t^n - |\mathbf{x} - \mathbf{y}|; \mathbf{x}, \mathbf{y} \in T\}$.
Alternative Approximation I. The outer integral is approximated by the midpoint rule, while the inner integral is evaluated using the three point rule for singular integrals. This gives

$$\begin{aligned}\int_T \int_T \frac{\partial_t c_T(t^n - |\mathbf{x} - \mathbf{y}|)}{|\mathbf{x} - \mathbf{y}|}\, ds_{\mathbf{y}}\, ds_{\mathbf{x}} &\approx \operatorname{gram} \Phi_T \int \frac{\partial_t c_T(t^n - |\mathbf{x_T} - \mathbf{y}|)}{|\mathbf{x_T} - \mathbf{y}|}\, ds_{\mathbf{y}} \\ &\approx (\operatorname{gram} \Phi_T)^2 \sum_{i=1}^{3} \theta_i \frac{\partial_t c_T(t^n - |\mathbf{x_T} - \Phi_T(\eta_i)|)}{|\mathbf{x_T} - \mathbf{\Phi_T}(\eta_i)|},\end{aligned}$$

where (η_i, θ_i) are the integration points on T_{ref} with the corresponding weights. The term $c_T(t^n - |\mathbf{x_T} - \Phi_T(\eta_i)|)$ can be evaluated again by interpolating between integer multiples of Δt. As can be seen in figure 19 this approximation leads to an extremely unstable scheme.
Alternative Approximation II. The outer integral is approximated by the seven point Gauss rule. Then seven singular integrals have to be approximated. These seven integrals are evaluated using a 27–point rule for singular integrals, i.e.

$$\begin{aligned}\int_T \int_T \frac{\partial_t c_T(t^n - |\mathbf{x} - \mathbf{y}|)}{|\mathbf{x} - \mathbf{y}|}\, ds_{\mathbf{y}}\, ds_{\mathbf{x}} &\approx \operatorname{gram} \Phi_T \sum_{i=1}^{7} \omega_i \int \frac{\partial_t c_T(t^n - |\Phi_T(\xi_i) - \mathbf{y}|)}{|\Phi_T(\xi_i) - \mathbf{y}|}\, ds_{\mathbf{y}} \\ &\approx (\operatorname{gram} \Phi_T)^2 \sum_{i=1}^{7} \sum_{j=1}^{27} \omega_i \sigma_i \frac{\partial_t c_T(t^n - |\Phi_T(\xi_i) - \Phi_T(\eta_j)|)}{|\Phi_T(\xi_i) - \mathbf{\Phi_T}(\eta_j)|},\end{aligned}$$

with (ξ_i, ω_i) being the Gauss–points on T_{ref} with the corresponding weights. As before, the resulting scheme is extremely unstable. This behaviour is caused by the very small entries in Q^0.
Remark. In this approach the mesh–ratio r cannot be chosen arbitrarily. If it was too small, the matrix Q^0 would be identically zero and no time–stepping algorithm could be derived from the approximation. For approximation I., r should be bigger than $\sqrt{2}/12$. This is not a big constraint since - as explained in section 3.2 - small meshratios lead to wrong solutions.

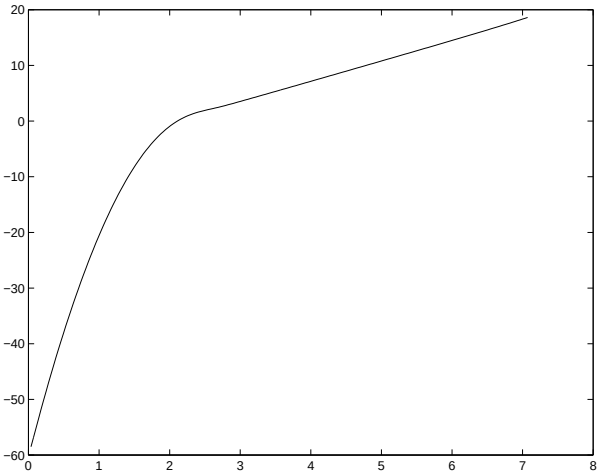

Figure 19: Logarithm of the L^2–norm for the alternative approximation I, $r = 0.6$

3.6 $(P1, P1)$–Discretization

In this section it will be shown how the bilinear form (17) discretizes for functions that are piecewise affine–linear, globally continuous in both, space and time. The discrete space $V_{\mathcal{T},\Delta t}$ is now

$$V_{\mathcal{T},\Delta t} = \{f; \quad f(\mathbf{x},t) = \sum_{i=0}^{N}\sum_{j=1}^{N_V} c_j^i \psi_i(t)\phi_j(\mathbf{x}), (c_j^i) \in \mathbb{R}^{N_N \times (N+1)}\},$$

where N_N is the number of nodes in $\mathcal{T}$ and ϕ_j are the nodal basis functions with respect to the triangulation $\mathcal{T}$. Let $f \in V_{\mathcal{T},\Delta t}$ with coefficients (c_j^i) and define $c_j(t) := \sum_{i=0}^{N} c_j^i \psi_i(t)$. As in the situation for spatially piecewise constant basis functions, it suffices to calculate $a(\phi_m\psi_n, f)$. It is

$$\begin{aligned}
a(\phi_m\psi_n, f) &= \int_0^\infty e^{-2\sigma t}\int_{\tilde{P}}\int_{\tilde{P}} \psi_n(t)\phi_m(\mathbf{x})\frac{\partial_t f(\mathbf{y}, t-|\mathbf{x}-\mathbf{y}|)}{|\mathbf{x}-\mathbf{y}|}\, ds_{\mathbf{y}}\, ds_{\mathbf{x}}\, dt \\
&\approx 2\Delta t e^{-2\sigma t^n}\int_{\tilde{P}}\int_{\tilde{P}} \psi_n(t^n)\phi_m(\mathbf{x})\frac{\partial_t f(\mathbf{y}, t^n-|\mathbf{x}-\mathbf{y}|)}{|\mathbf{x}-\mathbf{y}|}\, ds_{\mathbf{y}}\, ds_{\mathbf{x}} \\
&= 2\Delta t e^{-2\sigma t^n}\int_{\tilde{P}}\int_{\tilde{P}} \phi_m(\mathbf{x})\frac{\partial_t f(\mathbf{y}, t^n-|\mathbf{x}-\mathbf{y}|)}{|\mathbf{x}-\mathbf{y}|}\, ds_{\mathbf{y}}\, ds_{\mathbf{x}} \\
&= 2\Delta t e^{-2\sigma t^n}\sum_{j=1}^{N_K}\left(\int_{\tilde{P}}\int_{\tilde{P}} \frac{\phi_m(\mathbf{x})\phi_j(\mathbf{y})\partial_t c_j(t^n-|\mathbf{x}-\mathbf{y}|)}{|\mathbf{x}-\mathbf{y}|}\, ds_{\mathbf{y}}\, ds_{\mathbf{x}}\right).
\end{aligned}$$

Let $\operatorname{supp}\phi_m = \bigcup_{l=1}^{N_m} T_l$. The integral in the brackets is now calculated for all patches T_l, $l = 1, ..., N_m$, i.e.

$$\int_{T_l}\int_{\tilde{P}} \frac{\phi_m(\mathbf{x})\phi_j(\mathbf{y})\partial_t c_j(t^n-|\mathbf{x}-\mathbf{y}|)}{|\mathbf{x}-\mathbf{y}|}\, ds_{\mathbf{y}}\, ds_{\mathbf{x}} = \sum_{r=1}^{|\mathcal{T}|}\int_{T_l}\int_{T_r} \frac{\phi_m(\mathbf{x})\phi_j(\mathbf{y})\partial_t c_j(t^n-|\mathbf{x}-\mathbf{y}|)}{|\mathbf{x}-\mathbf{y}|}\, ds_{\mathbf{y}}\, ds_{\mathbf{x}}.$$

For $r \neq l$ the integrals are approximated by 3–point Gauss rules, i.e.

$$\begin{aligned}
&\int_{T_l}\int_{T_r} \frac{\phi_m(\mathbf{x})\phi_j(\mathbf{y})\partial_t c_j(t^n-|\mathbf{x}-\mathbf{y}|)}{|\mathbf{x}-\mathbf{y}|}\, ds_{\mathbf{y}}\, ds_{\mathbf{x}} \\
\approx &\sum_{\alpha=1}^{3}\sum_{\beta=1}^{3} \operatorname{gram}\Phi_l \operatorname{gram}\Phi_r \omega_\alpha\omega_\beta \frac{\phi_m(\Phi_l(\xi_\alpha))\phi_j(\Phi_r(\xi_\beta))\partial_t c_j(t^n-|\Phi_l(\xi_\alpha)-\Phi_r(\xi_\beta)|)}{|\Phi_l(\xi_\alpha)-\Phi_r(\xi_\beta)|},
\end{aligned}$$

while for $r = l$ the outer integral is approximated again by a Gauss 3–point rule and the inner ones by 3–point quadrature rules for singular integrals, i.e.

$$\begin{aligned}
&\int_{T_l}\int_{T_l} \frac{\phi_m(\mathbf{x})\phi_j(\mathbf{y})\partial_t c_j(t^n - |\mathbf{x}-\mathbf{y}|)}{|\mathbf{x}-\mathbf{y}|}\, ds_{\mathbf{y}}\, ds_{\mathbf{x}} \\
\approx\ & \partial_t c_j(t^n) \sum_{\alpha=1}^{3}\sum_{\beta=1}^{3} \operatorname{gram}\Phi_l \operatorname{gram}\Phi_l \omega_\alpha\theta_\beta \frac{\phi_m(\Phi_l(\xi_\alpha))\phi_j(\Phi_l(\eta_\beta))}{|\Phi_l(\xi_\alpha)-\Phi_l(\eta_\beta)|}.
\end{aligned}$$

The linear form (18) gives

$$\begin{aligned}
\int_0^\infty e^{-2\sigma t}\int_{\tilde{P}} \psi_n(t)\phi_m(\mathbf{x})\partial_t g(\mathbf{x},t)\, ds_{\mathbf{x}}\, dt &\approx 2\Delta t e^{-2\sigma t^n}\int_{\tilde{P}} \phi_m(\mathbf{x})\partial_t g(\mathbf{x},t^n)\, ds_{\mathbf{x}}\, dt \\
&= 2\Delta t \sum_{l=1}^{N_m}\sum_{\alpha=1}^{3} \operatorname{gram}\Phi_l \omega_\alpha \phi_m(\Phi_l(\xi_\alpha))\partial_t g(\Phi_l(\xi_\alpha),t^n).
\end{aligned}$$

Again, after performing an integration in time and evaluating terms $c_j(t^n - |\Phi_l(\xi_\alpha) - \Phi_r(\xi_\beta)|)$ interpolating between integer multiples of Δt, the above approximations lead to a time-stepping scheme of the form

$$Q^0\mathbf{c}^n = \mathbf{b}^n - \sum_{m=1}^{n-1} Q^m \mathbf{c}^{n-m}.$$

All tested meshratios for the Gaussian pulse $g(\mathbf{x},t) = \exp(-10(t-2.5)^2)$ were stable.

3.7 Convergence Results for a special Forcing Function

Bamberger and Duong state in [BaDuo] the following theorem to estimate the error of the Galerkin–solution. This theorem does not take account of the approximation of the surface.

Theorem 8 *If the solution ϕ of the retarded potential integral equation satisfies the regularity condition*

$$\phi \in H^2_\sigma(\mathbb{R}_{>0}, H^{m_1+1}(\Gamma)) \cap H^{m_2+1}_\sigma(\mathbb{R}_{>0}, L^2(\Gamma))$$

then there exists a constant C such that

$$|\phi - \phi_{h,\Delta t}|_{\sigma,-1/2,-1/2} \le C\left| |g'_{h,\Delta t} - g'|_{\sigma,-1/2,-1/2} + h^{m_1+\frac{1}{2}}|\phi|_{\sigma,2,m_1} + \frac{\Delta t^{m_2}}{\sqrt{h}}|\phi|_{\sigma,m_2+1,0}\right|,$$

where $g'_{h,\Delta t}$ is the approximation of g' with respect to the chosen basis–functions, $\phi_{h,\Delta t}$ the Galerkin approximation, m_1 the polynomial degree of the spatial basis–functions and m_2 the degree of the approximation in time.

Remark. For a discretization by functions that are piecewise constant in space ($m_1 = 0$) and piecewise affine–linear in time ($m_2 = 1$) a convergence rate $1/2$ is expected. This also shows that the quadratures have to be carried out with an appropriate exactness.
To analyze convergence of the schemes for solving the retarded potential integral equation, the forcing function is taken to be

$$g(\mathbf{x},t) := \int_{[0,1]^2} \frac{u(\mathbf{y}, t-|\mathbf{x}-\mathbf{y}|)}{|\mathbf{x}-\mathbf{y}|}\, ds_{\mathbf{y}},$$

where $u(\mathbf{x},t) = \max(0,t)$ so that the discrete solution should be $U(\mathbf{x},t) = \sum_{n=0}^{N} n\Delta t\psi_n(t)$. The function g can be evaluated similarly to the analytical calculation of the self–patch integral. The unit square is devided into four squares such that each square has the singularity at one vertex. Transforming the resulting integrals to polar–coordinates allows to evaluate them exactly. Figure 20 shows the temporal behaviour of the relative error with respect to the L^2–norm in space for the Galerkin Scheme using piecewise constant basis functions

and halfed squares of size h for the triangulation $\mathcal{T}$. The meshratio is fixed but different values of h are used. The bad behaviour of the error in the first time–steps is caused by the approximation of the self–patch and the non–smoothness of u at $t = 0$. The convergence rate at a fixed time is shown in figure 21 and is with 2.5 more than one can expect. Convergence results for piecewise affine–linear Ansatz–functions for the same example are shown in figures 22 and 23. Here the convergence rate at a fixed time is only 0.22 and worse than the one obtained for spatially piecewise constant elements. This might have two reasons. For both approximations the same quadrature rule is used, though for the $(P1, P1)$–discretization a higher one seems to be reasonable. In the simple selfpatch–approximation more information gets lost in the $P1$ situation than in the $P0$ situation.
Since the retarded potential integral equation will later be considered together with certain boundary conditions, in a second experiment for spatially affine linear functions, the boundary values $u = t$ are imposed on the edges $[0, 1] \times \{0, 1\}$. Here the convergence rate is 0.4 (compare figures 24 and 25).

3.8 A numerically cheaper Algorithm

The collocation method presented in section 3.1 is in fact a Galerkin scheme, when the integrals over the triangles are approximated by the midpoint rule. As shown, the resulting scheme is extremely unstable. The advantage of that scheme in comparison to the presented Galerkin scheme are the numerical costs. The scheme with the Gauss-three point approximation is about nine times as expensive as the direct scheme. The question that arises, is whether it is necessary to approximate all integrals that apppear in the Galerkin–discretization by a high quadrature rule. Since the coefficients $C_{T,T'}$ are bigger for triangles T' close to T than for triangles T' at a bigger distance, the idea is to approximate the integrals

$$\int_T \int_{T'} \frac{\partial_t c_T(\mathbf{y}, t - |\mathbf{x} - \mathbf{y}|)}{|\mathbf{x} - \mathbf{y}|} \, ds_{\mathbf{y}} ds_{\mathbf{x}}$$

by applying the Gauss rule to both integrals, if T and T' are close together and by the midpoint rule else. For a meshratio $r = 0.6$ it suffices to do the higher integration for $|\mathbf{x}_T - \mathbf{x}_{T'}| < 1/3$ to stabilize the example from section 3.1 while for $r = 0.8$ ($r = 1.1$, $r = 1.3$) a radius 0.38 (0.5, 0.6) is sufficient.

3.9 Results for a curved Surface

The numerical stability analysis has only been carried out for flat plates. In this section, the results for the part of the unit sphere

$$P = \{(\cos\phi\cos\psi, \sin\phi\cos\psi, \sin\psi), \phi \in [0, 0.94\pi/2], \psi \in [0, \pi/2]\}$$

are presented. P is discretized into 324 flat triangles as shown in figure 27. The selfpatch–integral is approximated by the 12–point rule from section 3.3. For the Galerkin scheme all tested meshratios were stable. Figures 28 and 29 show the solution for $g(\mathbf{x}, t) = \exp(-(t - 2.5)^2)$ after one and after 500 time–steps for a scheme with $r > 1$ ($\Delta t = 0.019$) while figures 30 and 31 show the numerical solution after 162 and after 190 time–steps for a scheme with $r < 1$ ($\Delta t = 0.017$).

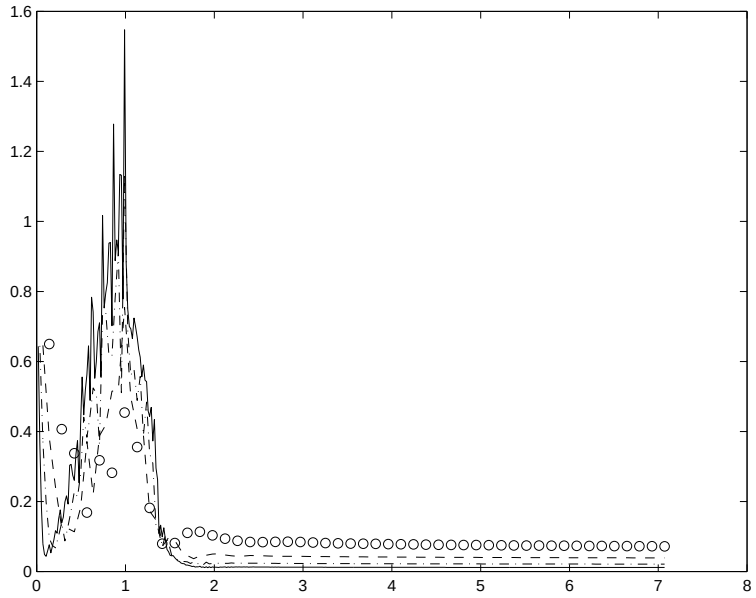

Figure 20: Behaviour of the relative error for $P0$-elements, $r = 0.6$ for $h = 1/2$ (circles), $h = 1/4$ (- -), $h = 1/8$ (- · -) and $h = 1/16$ (—)

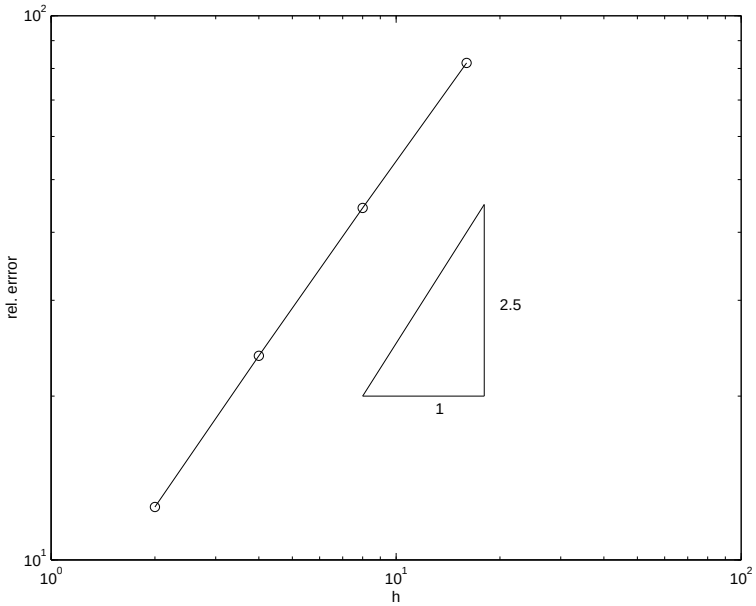

Figure 21: Double–logarithmic relative error for $P0$-elements at time $t = 4$

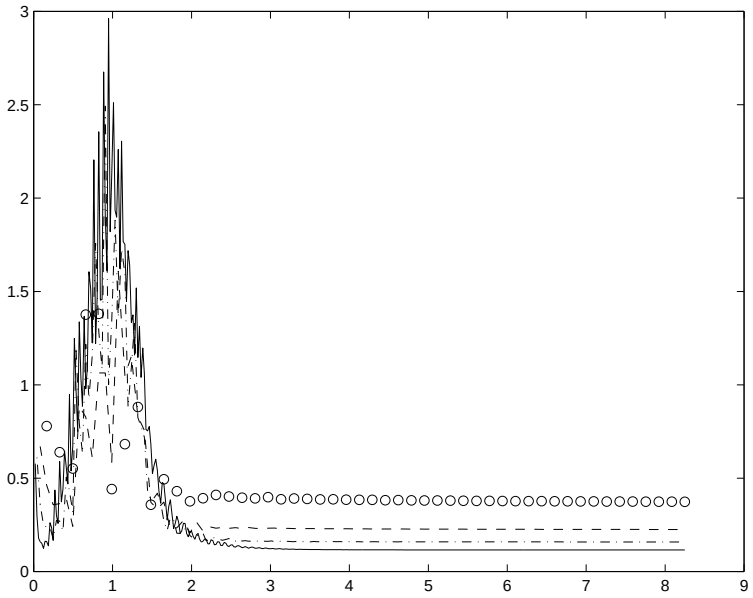

Figure 22: Behaviour of the relative error for $P1$-elements, $r = 0.6$ for $h = 1/2$ (circles), $h = 1/4$ (- -), $h = 1/8$ (- · -) and $h = 1/16$ (—)

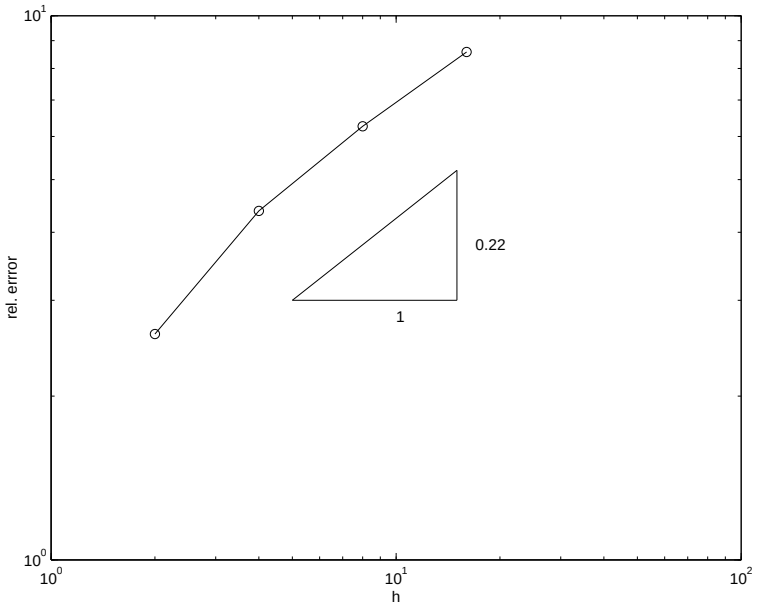

Figure 23: Double–logarithmic relative error for $P1$-elements at time $t = 4$

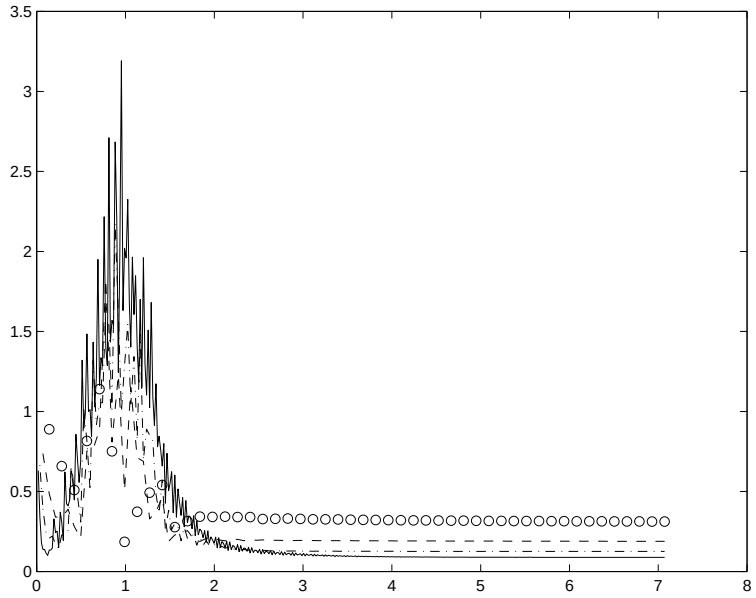

Figure 24: Behaviour of the relative error for $P1$-elements with boundary conditions, $r = 0.6$ for $h = 1/2$ (circles), $h = 1/4$ (- -), $h = 1/8$ (- · -) and $h = 1/16$ (—)

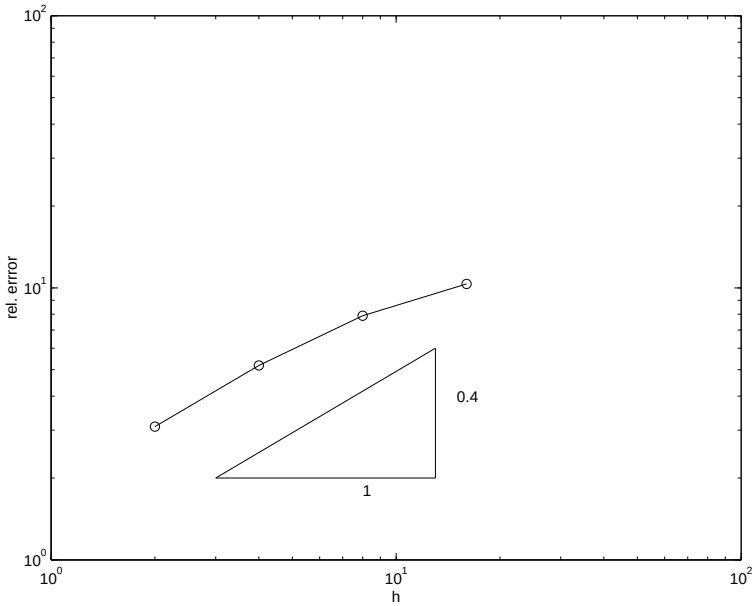

Figure 25: Double–logarithmic relative error for $P1$-elements with boundary conditions at time $t = 4$

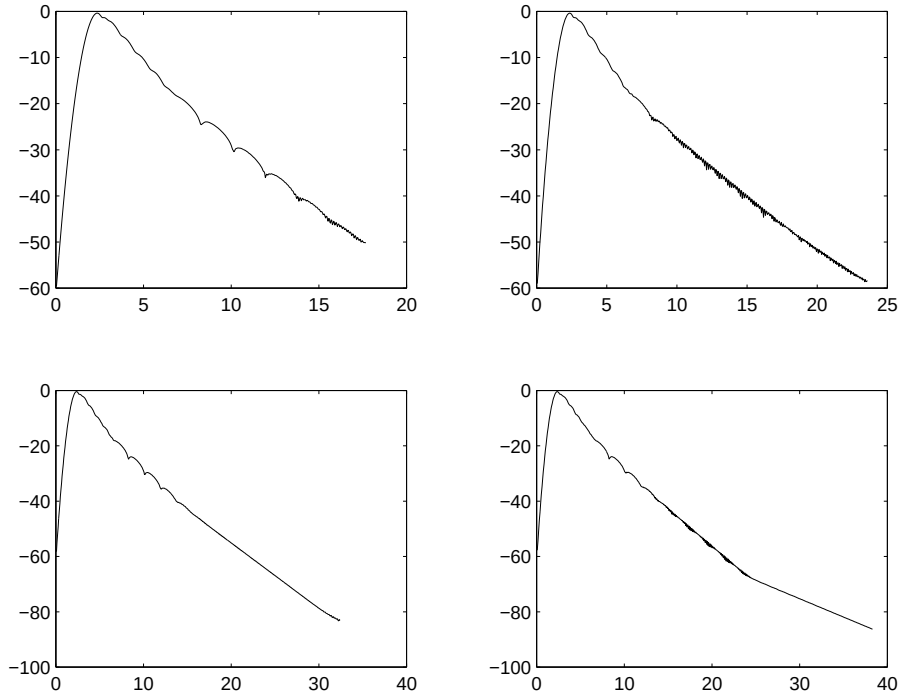

Figure 26: Results for the numerically cheaper algorithm, $r = 0.6, 0.8, 1.1, 1.3$

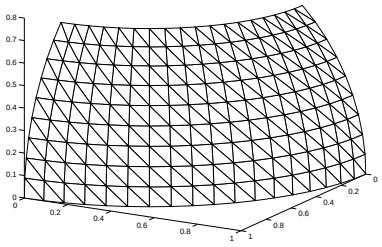

Figure 27: Triangulation of P

4 Schemes for the full Problem

As mentioned before, the retarded potential integral equation makes algorithms for solving the full problem unstable. To illustrate this difficulty, a simplified situation is considered. The scatterer is assumed to be a flat plate $P \subset \mathbb{R}^2 \times \{0\}$. This simplifies the mathematical formulation, since the surface divergence is the usual two–dimensional divergence operator and the tangential component of a vector–field $\mathbf{T} = (T_1, T_2, T_3)$ relative to P is given by $\mathbf{T}_{tan} = (T_1, T_2)$. The condition that the current is a tangential vector–field thus means that the third component is zero. Since most interest lies in stability effects, the assumption that the tangential component and the surface divergence can be calculated exactly, seems not to be a big constraint. Again, the equations are nondimensionalised such that the speed of light is equal to unity.

4.1 An Algorithm for rectangular Plates

When the edges of the plate P are parallel to the axes, it is possible to derive a simple algorithm. Let $P = [-1/2, 1/2]^2 \times \{0\}$. A determining set of equations to calculate the potentials $\mathbf{A} = (A_1, A_2, 0)$, ϕ and

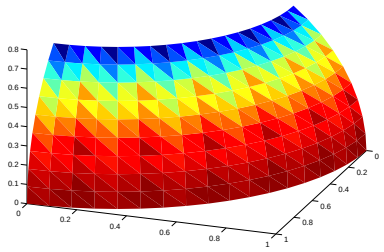

Figure 28: First solution for $r > 1$

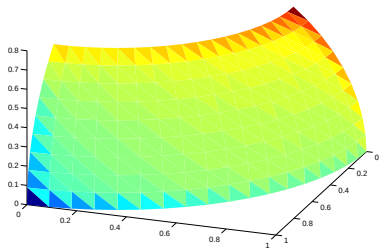

Figure 29: Solution after 500 time–steps for $r > 1$

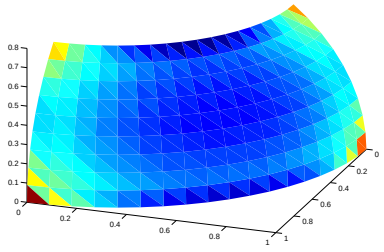

Figure 30: Solution after 162 time–steps for $r < 1$

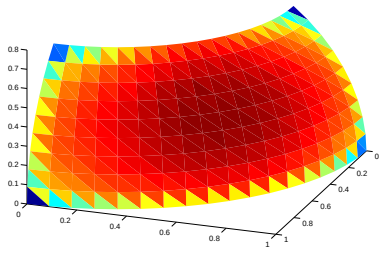

Figure 31: Solution after 190 time–steps for $r < 1$

the current $\mathbf{j} = (j_1, j_2, 0)$ due to an incident field $\mathbf{E}^{inc} = (E_1^{inc}, E_2^{inc}, E_3^{inc})$ is the Lorentz–Gauge condition together with the electric field integral equation and the vector retarded potential integral equation, i.e.

$$\frac{\partial}{\partial x_1} A_1 + \frac{\partial}{\partial x_2} A_2 = -\frac{\partial}{\partial t}\phi \tag{27}$$

$$\frac{\partial}{\partial x_1}\phi + \frac{\partial}{\partial t} A_1 = E_1^{inc} \tag{28}$$

$$\frac{\partial}{\partial x_2}\phi + \frac{\partial}{\partial t} A_2 = E_2^{inc} \tag{29}$$

$$A_1(\mathbf{x}, t) = \frac{1}{4\pi}\int_P \frac{j_1(\mathbf{y}, t - |\mathbf{x}-\mathbf{y}|)}{|\mathbf{x}-\mathbf{y}|}\, ds_{\mathbf{y}} \tag{30}$$

$$A_2(\mathbf{x}, t) = \frac{1}{4\pi}\int_P \frac{j_2(\mathbf{y}, t - |\mathbf{x}-\mathbf{y}|)}{|\mathbf{x}-\mathbf{y}|}\, ds_{\mathbf{y}} \tag{31}$$

in $P \times \mathbb{R}_{>0}$ together with the boundary condition

$$\mathbf{j} \cdot \tilde{\mathbf{n}} = 0 \quad \text{on } \partial P \text{ or}$$
$$j_1 = 0 \text{ on } \{-1/2, 1/2\} \times [-1/2, 1/2], \qquad j_2 = 0 \text{ on } [-1/2, 1/2] \times \{-1/2, 1/2\} \tag{32}$$

and the initial condition

$$\mathbf{j} = \mathbf{A} = \phi = 0, \quad t \le 0. \tag{33}$$

When $\mathbf{A}$ and ϕ are known, the scattered field is obtained from the relation $\mathbf{E}^{scat} = -\mathrm{grad}\,\phi - \frac{\partial}{\partial t}\mathbf{A}$. For the basic algorithm by Rynne (see [RySm],[Da2]), P is descretized uniformly into N^2 squares T_l of side $1/N$ with edges E_i^x parallel to the x–axis and E_i^y parallel to the y–axis. Let R_l denote the set of squares whose vertices are midpoints of the edges E_i^x and S_l the squares spanned by midpoints of the edges E_i^y. Moreover let Q_l denote the squares spanned by midpoints of the T_l (compare figure 32). The discretization of the time interval $[0, T]$ is uniform with step–size Δt. The unknown quantities ϕ, A_1 and A_2 are approximated by functions that are piecewise polynomial of partial degree less or equal one on each Q_l, R_l and S_l respectively, globally continuous in space and piecewise affine linear, globally continuous in time while $\mathbf{j}$ is approximated piecewise constant on squares around the nodes for $\mathbf{A}$ but piecewise affine linear, globally continuous in time. The approximations are

$$a(\mathbf{x}, t) = \sum_{n=0}^{M}\sum_i a^n_{(NM_{E_x^i})}\psi_n(t)\varphi_i^R(\mathbf{x})$$

for A_1, where φ_i^R are the nodal basis functions for the vertices of the squares R_l which are the midpoints of edges parallel to the x–axis, denoted by $M_{E_x^i}$,

$$b(\mathbf{x}, t) = \sum_{n=0}^{M}\sum_i b^n_{(NM_{E_y^i})}\psi_n(t)\varphi_i^S(\mathbf{x})$$

for A_2, where φ_i^S are the nodal basis functions for the vertices of the squares S_l which are the midpoints of edges parallel to the y–axis, denoted by $M_{E_y^i}$,

$$c(\mathbf{x}, t) = \sum_{n=0}^{M}\sum_i c^n_{(NM_{T_i})}\psi_n(t)\varphi_i^Q(\mathbf{x}),$$

for ϕ, where φ_i^Q are the nodal basis functions for the vertices of the squares Q_l which are the centres of the squares T_l, denoted by M_{T_i}.

Equation (27) is evaluated at midpoints of the squares T_l, equation (28) at those of the R_l and (29) at the centres of the S_l. The involved time–derivatives are approximated by two–step central differences and the spatial derivatives are given by central differences since the spatial basis functions are affine linear on the associated edges. All equations are considered at integer multiples of Δt, i.e.

$$c^n_{j-1/2,k-1/2} = c^{n-2}_{j-1/2,k-1/2} + 2r\left\{(S_x^{-1} - 1)a^{n-1}_{j,k-1/2} + (S_y^{-1} - 1)b^{n-1}_{j-1/2,k}\right\}$$

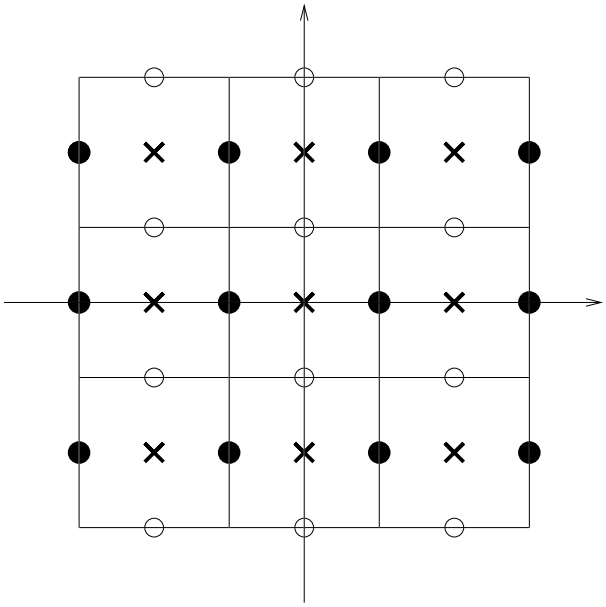

Figure 32: Staggered grid for the square $[-1/2,1/2]^2$, nodes for A_1 are the filled circles, for A_2 the open circles and for ϕ the crosses

for $1-N/2 \le j,k \le N/2$,

$$a^n_{j,k-1/2} = a^{n-2}_{j,k-1/2} + 2\Delta t d^{n-1}_{j,k-1/2} + \frac{r}{2}(1-S_x)\left\{c^{n-2}_{j-1/2,k-1/2} + 2c^{n-1}_{j-1/2,k-1/2} + c^n_{j-1/2,k-1/2}\right\}$$

for $-N/2 \le j \le N/2$ and $1-N/2 \le k \le N/2$ with $d^{n-1}_{j,k-1/2} := E^{inc}_1(\frac{1}{N}(j,k-1/2),(n-1)\Delta t)$, and

$$b^n_{j-1/2,k} = b^{n-2}_{j-1/2,k} + 2\Delta t e^{n-1}_{j-1/2,k} + \frac{r}{2}(1-S_y)\left\{c^{n-2}_{j-1/2,k-1/2} + 2c^{n-1}_{j-1/2,k-1/2} + c^n_{j-1/2,k-1/2}\right\}$$

for $1-N/2 \le j \le N/2$ and $-N/2 \le k \le N/2$ with $e^{n-1}_{j-1/2,k} := E^{inc}_2(\frac{1}{N}(j,k-1/2),(n-1)\Delta t)$. From these equations, $\mathbf{A}^n$, ϕ^n not on the edge of P can be found from $\mathbf{A}^i$, ϕ^i and E^{inc}, $i = n-2, n-1$. The values of $\mathbf{A}^n$ on ∂P are calculated from the retarded potential integral equations. In this step j^n_1 (j^n_2) is only needed on $\{-1/2,1/2\}\times[-1/2,1/2]$ ($[-1/2,1/2]\times\{-1/2,1/2\}$) but there j_1 (j_2) is zero for all n by the boundary condition (32).

Collocation–method for the current. When $\mathbf{A}^n$ is known, $\mathbf{j}^n$ is found using a collocation method similar to the one described in section 3.1. This basic algorithm is unstable for meshratios $r < 0.65$ as can be seen from figures 33 and 34 where the incident field is $\mathbf{E}^{inc} = (0, -\exp(-(t-3.4)^2), 0)$ and $r = 0.4$.

Averaging the current. In [Da2] an averaging–step for the current $\mathbf{j}$ is introduced to improve the stability of the scheme. This step works as follows: Assume that all quantities are calculated up to t^{n-1}. Then find the temporal quantities $\tilde{\mathbf{j}}^n$ and $\tilde{\mathbf{j}}^{n+1}$ from the basic scheme described before. The averaged current is then $\mathbf{j}^n = \frac{1}{4}\left(\mathbf{j}^{n-1} + 2\tilde{\mathbf{j}}^n + \tilde{\mathbf{j}}^{n+1}\right)$. Stability of this averaged algorithm can be shown numerically by a Fourier–analysis similar to the one carried out for the retarded potential integral equation in section 3.4. The stable averaged solution of the above example is shown in figure 35.

Galerkin–method for the current. As a third alternative, $\mathbf{j}^n$ is found from $\mathbf{A}^n$ discretizing the retarded potential integral equation by the Galerkin method from section 3.2. This method stabilizes the example, too (compare figure 36). The solutions from the averaging method and the Galerkin method in the interval $n \in [1000, 1100]$ for J_2 at the centre of the plate are compared in figure 37. The oscillations in the Galerkin solution are about ten times as big as for the averaged solution.

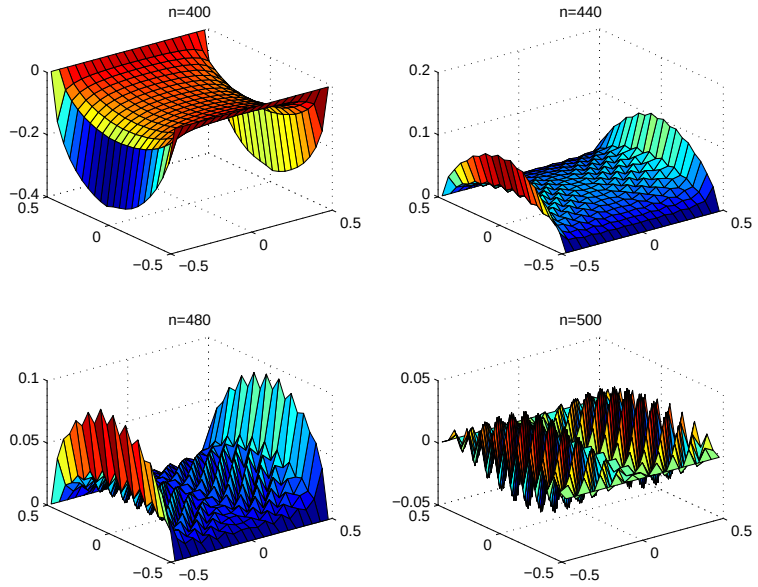

Figure 33: Arising of an instability in the solution j_2 for the collocation method

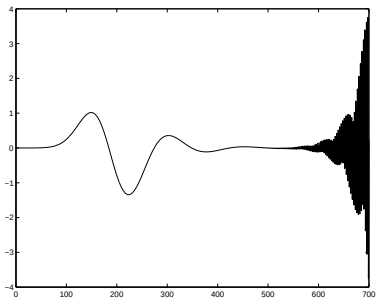

Figure 34: j_2 at the centre of the plate grows exponentially

4.2 Galerkin–Scheme for the Electric Field Integral Equation

For the Galerkin scheme for the full problem a general flat plate $P \subset \mathbb{R}^2 \times \{0\}$ is considered. Let $\mathcal{T}$ be a regular triangulation of P. To discretize the bilinear form (19) a discrete subspace which satisfies the boundary conditions is

$$V_{\mathcal{T},\Delta t} = \left\{ \mathbf{f}, \quad \mathbf{f}(\mathbf{x},t) = \sum_{i=0}^{N} \sum_{j=1}^{2N_N} c_j^i \psi_i(t) \phi_j(\mathbf{x}), (c_j^i)_{0 \le i \le N, 1 \le j \le 2N_N} \in \mathbb{R}^{(N+1)\times 2N_N}, \mathbf{f} \cdot \tilde{\mathbf{n}} = 0 \text{ on } \partial\tilde{P} \right\},$$

where $\phi_j \in \{(\varphi_i, 0, 0), (0, \varphi_i, 0), 1 \le i \le N_N\}$ and the φ_i are the usual scalar $P1$ nodal basis functions and N_N is the number of nodes in the triangulation $\mathcal{T}$. For the implementation of the boundary condition $\mathbf{f} \cdot \tilde{\mathbf{n}} = 0$ it is assumed that the closed path $L = \partial\tilde{P}$ can be written in the form $L = \bigcup_{j=1}^{S-1} \text{conv}\,[K_{i_j}, K_{i_{j+1}}] \cup \text{conv}\,[K_{i_S}, K_{i_1}]$ for the nodes $\{K_{i_j}\}$ on L. For an edge $\text{conv}\,[K_{i_j}, K_{i_{j+1}}]$ the condition is then implemented for K_{i_j}.
Let $\mathbf{f} \in V_{\mathcal{T},\Delta t}$ with coefficients (c_j^i) and set $c_j(t) := \sum_{i=0}^{N} c_j^i \psi_i(t)$. The main step in the discretization is the use of the definition of the surface gradient. It is

$$a_2(\psi_n \phi_m, \mathbf{f}) \quad = \quad \int_0^\infty e^{-2\sigma t} \left(\int_{\tilde{P}} \psi_n(t) \phi_m(\mathbf{x}) \frac{\partial}{\partial t} \int_{\tilde{P}} \frac{\mathbf{f}(\mathbf{y}, t - |\mathbf{x}-\mathbf{y}|)}{|\mathbf{x}-\mathbf{y}|} \, ds_{\mathbf{y}} \right.$$

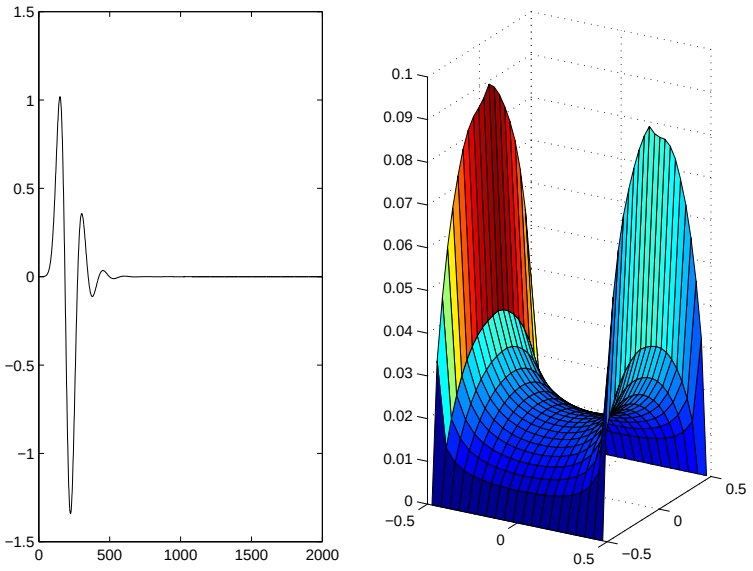

Figure 35: Results for the averaged solution. j_2 near the centre (left) and after 480 timesteps (right)

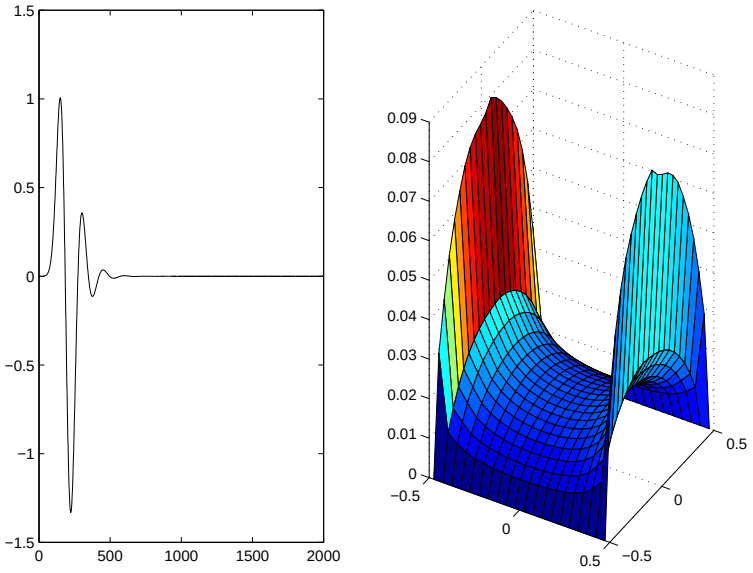

Figure 36: Results for the Galerkin solution. j_2 near the centre (left) and after 480 timesteps (right)

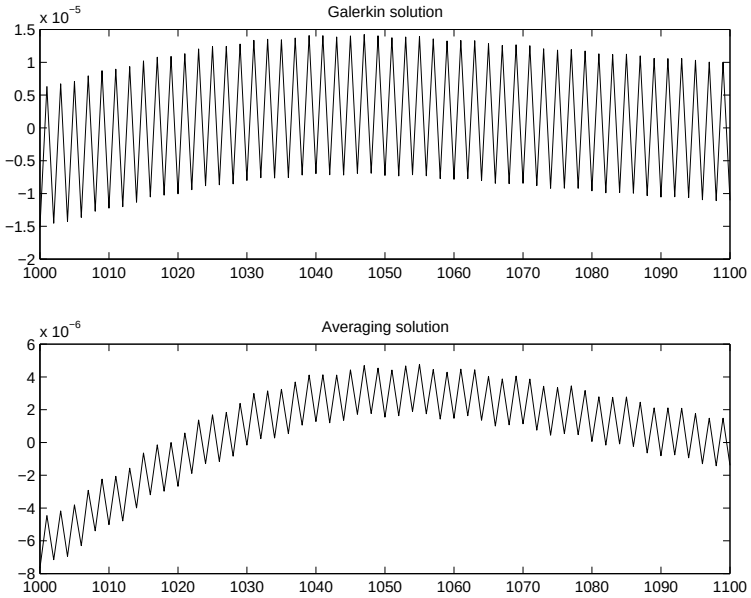

Figure 37: Comparison of j_2 at $(0,0)$

$$
\begin{aligned}
& -\psi_n(t)\phi_m(\mathbf{x})\mathrm{grad}_{\tilde{P}} \int_{\tilde{P}} \left(\int_0^{t-|\mathbf{x}-\mathbf{y}|} \mathrm{div}_{\tilde{P}} \mathbf{f}(\mathbf{y},\tau)\, d\tau \right) \frac{1}{|\mathbf{x}-\mathbf{y}|}\, ds_{\mathbf{y}}\, ds_{\mathbf{x}} \Bigg)\, dt \\
\approx\ & 2\Delta t e^{-2\sigma t^n} \left(\int_{\tilde{P}} \psi_n(t^n)\phi_m(\mathbf{x}) \frac{\partial}{\partial t} \int_{\tilde{P}} \frac{\mathbf{f}(\mathbf{y}, t^n - |\mathbf{x}-\mathbf{y}|)}{|\mathbf{x}-\mathbf{y}|}\, ds_{\mathbf{y}} \right. \\
& \left. -\psi_n(t^n)\phi_m(\mathbf{x})\mathrm{grad}_{\tilde{P}} \int_{\tilde{P}} \left(\int_0^{t^n-|\mathbf{x}-\mathbf{y}|} \mathrm{div}_{\tilde{P}} \mathbf{f}(\mathbf{y},\tau)\, d\tau \right) \frac{1}{|\mathbf{x}-\mathbf{y}|}\, ds_{\mathbf{y}}\, ds_{\mathbf{x}} \right) \\
=\ & 2\Delta t e^{-2\sigma t^n} \left(\int_{\tilde{P}} \phi_m(\mathbf{x}) \frac{\partial}{\partial t} \int_{\tilde{P}} \frac{\mathbf{f}(\mathbf{y}, t^n - |\mathbf{x}-\mathbf{y}|)}{|\mathbf{x}-\mathbf{y}|}\, ds_{\mathbf{y}} \right. \\
& \left. -\mathrm{div}_{\tilde{P}} \phi_m(\mathbf{x}) \int_{\tilde{P}} \left(\int_0^{t^n-|\mathbf{x}-\mathbf{y}|} \mathrm{div}_{\tilde{P}} \mathbf{f}(\mathbf{y},\tau)\, d\tau \right) \frac{1}{|\mathbf{x}-\mathbf{y}|}\, ds_{\mathbf{y}}\, ds_{\mathbf{x}} \right).
\end{aligned}
$$

The first part of the last sum is treated in the same way as the retarded potential integral equation in the $(P1,P1)$-version, where again the time dependent part is interpolated between integer multiples of Δt but gives, since the derivative is considered

$$
\frac{\partial}{\partial t} c_j(t^n - |\Phi_r(\xi_\alpha) - \Phi_r(\xi_\beta)|) = \left(c_j^{\,n-m_{\xi_\alpha^r,\xi_\beta^s}} - c_j^{\,n-m_{\xi_\alpha^r,\xi_\beta^s}-1} \right) / \Delta t.
$$

For the second part, the support of ϕ_m is divided into the patches $\mathrm{supp}\,\phi_m = \bigcup_{l=1}^{N_m} T_l$ and each patch T_l is treated seperately. For a triangle T_r the six basis functions that are not identically zero on T_r are denoted by ϕ_{r_κ}, $\kappa = 1,\ldots 6$. It is

$$
\begin{aligned}
& \int_{T_l} \int_{\tilde{P}} \mathrm{div}_{\tilde{P}} \phi_m \left(\int_0^{t^n-|\mathbf{x}-\mathbf{y}|} \mathrm{div}_{\tilde{P}} \mathbf{f}(\mathbf{y},\tau)\, d\tau \right) \frac{1}{|\mathbf{x}-\mathbf{y}|}\, ds_{\mathbf{y}}\, ds_{\mathbf{x}} \\
=\ & \sum_{r=1}^{|\mathcal{T}|} \int_{T_l} \int_{T_r} \mathrm{div}_{\tilde{P}} \phi_m \left(\int_0^{t^n-|\mathbf{x}-\mathbf{y}|} \mathrm{div}_{\tilde{P}} \mathbf{f}(\mathbf{y},\tau)\, d\tau \right) \frac{1}{|\mathbf{x}-\mathbf{y}|}\, ds_{\mathbf{y}}\, ds_{\mathbf{x}}
\end{aligned}
$$

$$
\begin{aligned}
&= \sum_{r=1}^{|\mathcal{T}|} \int_{T_l} \int_{T_r} \operatorname{div}_{\tilde{P}} \phi_m \left(\int_0^{t^n - |\mathbf{x}-\mathbf{y}|} \sum_{i=0}^{N} \sum_{j=1}^{2N_V} c_j^i \psi_i(\tau) \operatorname{div}_{\tilde{P}} \phi_j(\mathbf{y})\, d\tau \right) \frac{1}{|\mathbf{x}-\mathbf{y}|}\, ds_{\mathbf{y}}\, ds_{\mathbf{x}} \\
&= \sum_{r=1}^{|\mathcal{T}|} \int_{T_l} \int_{T_r} \operatorname{div}_{\tilde{P}} \phi_m \left(\int_0^{t^n - |\mathbf{x}-\mathbf{y}|} \sum_{i=0}^{N} \sum_{j=1}^{2N_V} c_j^i \psi_i(\tau) \operatorname{div}_{\tilde{P}} \phi_j(\mathbf{y})\, d\tau \right) \frac{1}{|\mathbf{x}-\mathbf{y}|}\, ds_{\mathbf{y}}\, ds_{\mathbf{x}} \\
&= \sum_{r=1}^{|\mathcal{T}|} \sum_{\kappa=1}^{6} \int_{T_l} \int_{T_r} \frac{\operatorname{div}_{\tilde{P}} \phi_m \operatorname{div}_{\tilde{P}} \phi_{r_\kappa}}{|\mathbf{x}-\mathbf{y}|} \left(\int_0^{t^n - |\mathbf{x}-\mathbf{y}|} \sum_{i=0}^{N} c_{r_\kappa}^i \psi_i(\tau)\, d\tau \right) ds_{\mathbf{y}}\, ds_{\mathbf{x}} \\
&=: \sum_{r=1}^{|\mathcal{T}|} \sum_{\kappa=1}^{6} \int_{T_l} \int_{T_r} \frac{\operatorname{div}_{\tilde{P}} \phi_m \operatorname{div}_{\tilde{P}} \phi_{r_\kappa}}{|\mathbf{x}-\mathbf{y}|} \psi_{r_\kappa}^*(t^n - |\mathbf{x}-\mathbf{y}|)\, ds_{\mathbf{y}}\, ds_{\mathbf{x}}.
\end{aligned}
$$

Since $\operatorname{div}_{\tilde{P}} \phi_j$ is constant on each triangle, the last expression can be treated as in section 3.2. Following those ideas, terms of the form $\psi_{r_\kappa}^*(t^n - |\xi_\alpha - \xi_\beta|)$, where ξ_α and ξ_β are quadrature points, appear. For these expressions it is

$$
\begin{aligned}
\psi_{r_\kappa}^*(t^n - |\xi_\alpha - \xi_\beta|) &= \int_0^{t^n - |\xi_\alpha - \xi_\beta|} \sum_{i=0}^{N} c_{r_\kappa}^i \psi_i(\tau)\, d\tau \\
&= \sum_{i=0}^{N} c_{r_\kappa}^i \int_0^{t^n - |\xi_\alpha - \xi_\beta|} \psi_i(\tau)\, d\tau
\end{aligned}
$$

and here the integrals of the temporal basis functions are approximated by

$$
\int_0^{t^n - |\xi_\alpha - \xi_\beta|} \psi_i(\tau)\, d\tau \approx \begin{cases} 0 & , \quad t^n - |\xi_\alpha - \xi_\beta| < (i-1)\Delta t \\ \Delta t & , \quad \text{else.} \end{cases}
$$

The linear form (20) is treated as in section 3.6 and these approximations again lead to a scheme of the form

$$
Q^0 \mathbf{c}^n = \mathbf{b}_2^n - \sum_{m=1}^{n-1} Q^m \mathbf{c}^{n-m}
$$

but here, in contrast to the scheme for the retarded potential integral equation, all previous time levels are involved. This is caused by the integral $\int_0^{t^n - |\Phi_r(\xi_\alpha) - \Phi_r(\xi_\beta)|} c_j(\tau)\, d\tau$. Figures 38 and 40 show a stable and an unstable solution for the unit square and the incident field from the previous section at meshratios $r = 0.6$ and $r = 0.9$. Here the mesh–size was $h = 1/8$ so that the time step size Δt is quite big and the solution does not show as many contours as in the previous section. It is not possible to say under what conditions the scheme is stable but a Fourier analysis similar to the one in section 3.4 could be carried out. Figure 39 shows the charge and the current for $h = 1/16$ after 10 time steps. Another example, where the plate is not rectangular is shown in figure 41.

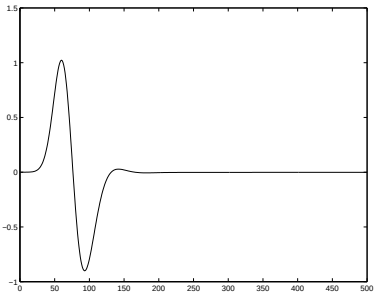

Figure 38: Numerical solution of the Galerkin scheme for the EFIE at $(0.5, 0.5)$

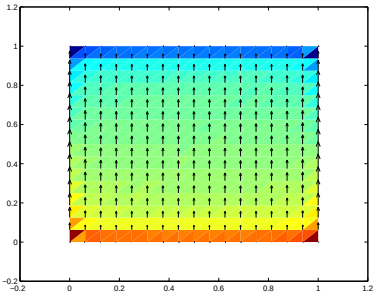

Figure 39: Charge and current for the stable example after 10 time steps

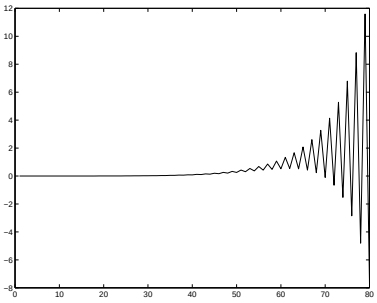

Figure 40: Unstable solution at $(0.5, 0.5)$

Acknowledgements

I am very grateful to D.B. Duncan, P.J. Davies and C. Carstensen for supervising me during this project. Moreover I would like to thank the Department of Mathematics of Heriot–Watt University for allowing me to attend the course.

References

[A] Adams, R.A., 'Sobolev Spaces', Pure Appl. Math. 65, Academic Press, New York, 1975.

[AlFi] Alonso, M. and Finn, E.J., 'Fundamental University Physics - Volume II, Fields and Waves', Addison–Wesley Publishing Company, 1967.

[BaDuo] Bamberger, A., Duong, T. Ha, 'Formulation Variationelle Espace-Temps por le Calcul par Potentiel Retardé de la Diffraction d'une Onde Acoustique (I)', Math. Meth. in the Appl. Sci. 8, 1986.

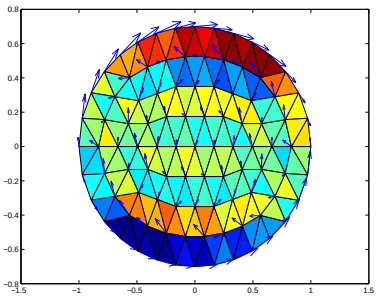

Figure 41: Charge and current after 40 time steps

[Da1] Davies, P.J., 'A stability analysis of a time marching scheme for the general surface electric integral equation', Applied Numerical Mathematics 27 (1998) 33-57.

[Da2] Davies, P.J., 'Stability of time-marching numerical schemes for the electric field integral equation', Journal of Electromagnetic Waves and Applications, Vol.8, No.1, 85-114,1994.

[Da3] Davies, P.J., 'Numerical stability and convergence of approximations of retarded potential integral equations', SIAM J. Numer. Anal., Vol. 31, No 3, 856-875, June 1994.

[Da4] Davies, P.J., 'On the Stability of Time-Marching Schemes for the General Surface Electric–Field Integral Equation', IEEE Transactions on Antennas and Propagation, Vol. 44, No 11, November 1996.

[DaDu] Davies, P.J., Duncan, D.B., 'Averaging techniques for time-marching schemes for retarded potential integral equations', Applied Numerical Mathematics 23 (1997) 291-310.

[Duf] Duffy, M.G., 'Quadrature over a Pyramid or cube of Integrands with a Singularity at a Vertex', SIAM J. Numer. Anal., Vol. 19, No 6, 1260-1262, December 1982.

[Jo] Jones, D.S., 'Theory of Electromagnetism', Oxford University Press, 1964.

[PeSi] Peirce, A., Siebrits, E., 'Stability Analysis and Design of Time–Stepping Schemes for General Elastodynamic Boundary Element Models', International Journal for Numerical Methods in Engineering', Vol. 40, 319-342 (1997).

[Pu] Pujols, A., 'Time Dependent Integral Method for Maxwell Equations', Math. and Num. Aspects of Wave Prop. Phenomena, Schönbourg, 1991.

[RySm] Rynne, B.P., Smith, P.D., 'Stability of Time Marching Algorithms for the Electric Field Integral Equation', Journal of Electromagnetic Waves and Applications, Vol. 4, No 12, 1181-1205, 1990.

[Wa] Wang, C.C., 'Mathematical Principles of Mechanics and Electromagnetism - Part B, Electromagnetism and Gravitation', Plenum Press, New York, 1979.